Spectroscopic characterization of thiol-derived self-assembling monolayers

2001 J. Phys.: Condens. Matter 13 11333

(http://iopscience.iop.org/0953-8984/13/49/314)

INSTITUTE OF PHYSICS PUBLISHING JOURNAL OF PHYSICS: CONDENSED MATTER

J. Phys.: Condens. Matter **13** (2001) 11333–11365 PII: S0953-8984(01)25182-0

Spectroscopic characterization of thiol-derived self-assembling monolayers

M Zharnikov[1] **and M Grunze**

Angewandte Physikalische Chemie, Universität Heidelberg, Im Neuenheimer Feld 253, D-69120 Heidelberg, Germany

E-mail: michael.zharnikov@urz.uni-heidelberg.de

Received 25 May 2001, in final form 5 July 2001
Published 10 December 2001
Online at stacks.iop.org/JPhysCM/13/11333

Abstract

This article reviews recent progress in the spectroscopic characterization of aliphatic and aromatic thiol-derived self-assembled monolayers (SAMs) on noble metal substrates. Several complementary techniques such as near edge x-ray absorption fine structure spectroscopy, x-ray photoelectron spectroscopy, and infrared reflection absorption spectroscopy were applied to study the balance between intermolecular and adsorbate–substrate interactions, chemical identity of the headgroup, and absorption site homogeneity at the sulphur–metal interface. Whereas in the thioaliphatic SAMs the headgroup–substrate interaction was found to be a decisive factor for the structure and packing in these films, these parameters are mainly determined by the intermolecular interactions in the thioaromatic films. Only one sulphur species could be detected in the S 2p HRXPS spectra of both aliphatic and aromatic SAMs suggesting binding of individual molecules as thiolates. Conclusions on the heterogeneity of the adsorption sites are derived and evidence that the investigated films represent highly correlated molecular assemblies are presented.

1. Introduction

Self-assembled monomolecular films consisting of relatively large, long-chain semiflexible organic molecules have recently attracted considerable interest in physics, chemistry and biology due to their ability to control wetting, adhesion, lubrication and corrosion on surfaces and interfaces [1, 2]. These films, called self-assembled monolayers (SAMs), are formed by 2D aggregation of amphiphilic molecules on a suitable substrate. The respective molecules consist of three units: a headgroup which binds strongly to the substrate, a tail group that constitutes the outer surface of the film, and a spacer that connects head and tail and effects the intermolecular separation, molecular orientation and the degree of order in the film. Providing

[1] Corresponding author.

that the tail group has a strong polar character or is sufficiently large it cannot only determine the properties of the outer film surface but also significantly affect its entire structure.

Among different kinds of SAMs, films formed from thiol-derived molecules on noble metal substrates, like Au and Ag, have been most extensively studied due to their stability and ease of fabrication [2, 3]. The primary emphasis was placed on SAMs of alkanethiols (AT or Cn: $CH_3(CH_2)_{n-1}SH$), although practically important [4–7] thioaromatic SAMs also attracted much attention throughout the last few years [4–17]. Nevertheless, many fundamental questions and practical issues concerning thiol-derived SAMs are still open. In our experiments we used several complementary spectroscopic techniques, like x-ray photoelectron spectroscopy (XPS), high resolution XPS (HRXPS), near edge x-ray absorption fine structure (NEXAFS) spectroscopy and infrared reflection absorption spectroscopy (IRRAS), to address some of these questions.

First, the importance of adsorbate–substrate and adsorbate–adsorbate interactions in the aliphatic and aromatic SAMs are addressed. It is well known that the lateral density and structure of SAMs are, to a large extent, the result of a delicate balance between these two interactions [1, 2, 18–20]. It is, however, generally believed that in the case of AT SAMs on (111)-oriented gold and silver substrates, the intermolecular interaction plays the predominant role [1, 2, 18, 21, 22]. The substrate is assumed to affect only the packing density of the AT moieties, through the corrugation of the sulphur–metal binding energy surface [1, 2, 18], which results in a dense and incommensurate structure for the thiolate headgroups on Ag (a lattice constant of ∼4.67–4.77 Å), and a commensurate lattice with a larger intersite spacing of ∼5.0 Å on Au [1, 2, 18, 19]. The packing observed on Ag is close to the most effective arrangement of the alkyl chains in a trigonal lattice with a lattice constant of ∼4.4 Å [1, 23], which is also reflected in a relatively small average tilt angle of 10–12° for the AT moieties [1, 2, 18, 21, 24]. In the less dense lattice on Au minimization of the lattice energy is achieved by tilting of the AT molecules by ∼27–35° [20, 21, 25–27]. Thus, the difference in the orientation of the AT molecules on Au and Ag is believed to be primarily related to the intermolecular van der Waals (vdW) interaction between the AT moieties [1, 2, 18]. In addition to this model, the hybridization of the sulphur headgroup was considered as an explanation for the change in orientation of the terminal methyl group with the number of CH_2 units in alkyl chain in AT SAMs on Au and Ag (odd-even effect) [28, 29]. An sp^3 bonding configuration of the chemisorbed sulphur headgroup on Au(111) and sp bonding on Ag(111) associated with surface-S-C angles of ∼104° and ∼180°, respectively, were proposed to account for inversion of the odd-even effect on Au and Ag [21, 28]. On the other hand, calculations suggest that there is no significant difference in energy between the sp^3 and sp hybridization of sulphur [18] and it is not clear from the available experimental data how important the hybridization of the sulphur headgroup is for the structure and lateral density in AT-like SAMs.

To reveal the role of the headgroup–substrate interaction in AT-like SAMs we used two different noble metal substrates (Au and Ag) and varied the strength and character of the chain–chain interaction. For the latter purpose we substituted the terminal methyl group of AT by a perfluoro nonane or by methylated biphenyl (BP) moiety and studied the resulting SAMs of semifluorinated alkanethiols $CF_3(CF_2)_9(CH_2)_nSH$ (SFAT or F10Hn, $n = 11, 17$) and 4,4′-biphenyl-substituted alkanethiols $CH_3(C_6H_4)_2(CH_2)_nSH$ (BPn, $n = 3$–6) on gold and silver substrates [30–32]. We also varied the strength and character of the headgroup substrate interaction in non-substituted AT SAMs by adsorbing mercury on the gold substrate [33].

In thioaromatic films, the relation between the intermolecular and headgroup–substrate interactions can be different than in AT SAMs. Compared to aliphatic chains, aromatic rings are characterized by larger vdW dimensions and interact with each other through both the vdW and electrostatic forces [34]. According to the melting points of benzene C_6H_6 (5.5 °C),

n-hexane C_6H_{14} (−95.3 °C), biphenyl $C_{12}H_{10}$ (69.0 °C), and n-dodecane $C_{12}H_{26}$ (−9.6 °C) [35], the intermolecular forces between the phenyl rings in aromatic systems are stronger than the vdW forces between the alkyl chains in aliphatic systems. However, this difference in the melting points may be largely related to entropic contributions, because the respective heats of sublimation are similar [34]. We studied SAMs formed from thiophenol (TP) C_6H_5SH, 1,1′-biphenyl-4-thiol (BPT) $H(C_6H_4)_2SH$, 1,1′;4′,1″-terphenyl-4-thiol (TPT) $H(C_6H_4)_3SH$, and anthracene-2-thiol (AnT) $C_{14}H_9SH$ on polycrystalline Au and Ag surfaces [36]. The choice of these particular systems allows the simultaneous variation of the most important parameters affecting the structure of thioaromatic SAMs, namely the length of the aromatic chain (TP against BPT against TPT), the rigidity and the character of the aromatic chain (AnT against BPT and TPT), and the substrate (Au against Ag). In this way, both the intermolecular and adsorbate–substrate interactions can be varied to study their effect on the film structure.

It should be mentioned that relatively little work has been done to clarify the structure of thioaromatic SAMs, especially on Ag substrates. For the simplest member of the arylthiols, thiophenol (TP), the detailed structure of the respective SAM on Au(111) surfaces has not been unambiguously determined: both well-ordered monolayers with an upright [37, 38] or strongly inclined [39] adsorption geometry of the phenyl rings and poorly defined films [8, 10, 11] were found. On Ag(111) surfaces, TP molecules seem to adsorb nearly perpendicular to the substrate surface [40, 41]. With a growing number of phenyl moieties in the aromatic chain, the monolayers become both more densely packed and well-ordered [4, 8, 10–12, 16], which can be associated with the increase of the intermolecular interactions mediated by the aromatic entities. As to the molecular arrangement, a herringbone packing is favoured [8–10, 12]. This packing is believed to be nearly the same on Au(111) and Ag(111) surfaces which should consequently result in similar monolayer structures [9]. For BPT SAMs on Au(111) molecular mechanics calculations [8] and recent x-ray diffraction data [17] implied a commensurate $(\sqrt{3} \times \sqrt{3})R30^\circ$ surface lattice. In contrast, neither periodic pattern nor molecularly resolved STM images were observed for this system [11], which can be explained by the difficulties in the preparation of high quality BPT SAMs on Au [17, 42].

The second principle question of our study was to clarify the nature of the adsorbate–substrate bond and to derive conclusions about the homogeneity of the adsorption sites in aliphatic and aromatic SAMs on the (111) surfaces of Au and Ag. Considerable theoretical and experimental efforts were made to clarify these issues and, in particular, identify the adsorbate–substrate bond. Both *ab initio* and semiempirical cluster calculations for short chain AT were performed [18, 43–45], and structural and spectroscopic experimental methods were applied [24, 27, 46–49]. However, there still are uncertainties about the chemical state and the geometrical structure at the SAM-substrate interface. In particular, both sulphur dimers with two sulphur atoms in non-equivalent adsorption sites and a commensurate $(\sqrt{3} \times \sqrt{3})R30^\circ$ lattice of the sulphur atoms in identical three-fold hollow sites were suggested for AT/Au, whereas an incommensurate $(\sqrt{7} \times \sqrt{7})R10.9^\circ$ lattice is generally assumed for sulphur in AT/Ag [1, 24, 27, 46, 49]. The chemical state of the sulphur headgroup on both Au and Ag is not explicitly known and even cleavage of the S–H bond upon the adsorption was recently questioned [44]. In comparison to AT SAMs, even less is known about the sulphur headgroups in BPT SAMs on Au and Ag except for the above-mentioned x-ray diffraction study by Leung *et al* [17].

To clarify the nature the adsorbate–substrate bond and to derive conclusions about the homogeneity of the adsorption sites in thiol-derived SAMs we applied synchrotron-based high-resolution x-ray photoelectron spectroscopy (HRXPS) to conventional aliphatic and aromatic SAMs [50] and to the 'aliphatic-aromatic' BPn films ($n = 1$–4) [51]. In addition, we studied the formation of SAMs from asymmetric dialkyl disulphides (ADDS or Cn-C16: $CH_3(CH_2)_{n-1}SS(CH_2)_{15}CH_3$, $n = 4$, 8, and 12) by several complementary spectroscopic

techniques [52, 53].

The variable excitation energy and high energy resolution of HRXPS allowed a precise characterization of the SAM–metal interface. The headgroup of the SAMs was monitored by using the S 2p core level. For the respective HRXPS spectra a relatively low excitation energies were selected because of the increase of the S 2p photoionization cross-section. Along with these spectra, we were interested in differences between the Au and Ag core levels of the bulk metal, the clean metal surface, and the metal atoms bonded to AT or BPT because no such differences have been measured so far. The major reason for the lack of data is presumably the limited energy resolution (not better than 0.4 eV) of previous HRXPS studies [16, 48, 54]. In our study we use an energy resolution of better than 0.1 eV, which allowed us to measure the intrinsic energy spread of the core-level photoemission process and monitor small binding energy (BE) shifts and differences.

The formation of SAMs formed from Cn-C16 allowed us to address the thiolate-versus-disulphide bonding issue by monitoring both Cn and C16 constituents upon the Cn-C16 adsorption. Generally, dialkyl disulphides (DDS) are well established as alternative precursors to AT for formation of SAMs on gold, silver or copper surfaces. Numerous reports show that the formation rates and film quality are similar for the two types of compounds [55–60]. At the same time DDS molecules offer potential advantages over AT molecules as SAM precursors. First, the disulphide group is more chemically stable than the thiol. Most important, the use of asymmetric dialkyl disulphides (ADDS; R_1SSR_2) is commonly believed to provide a means of achieving 1:1 asymmetric molecular arrangements via simultaneous incorporation of SR_1 and SR_2 into the growing SAM. Room temperature adsorption on gold results in homogeneously intermixed, two-component SAMs [60–62]. Annealing at $T = 100\,^{\circ}\mathrm{C}$ can produce phase segregation [62, 63]. The expected 1:1 stoichiometry of ADDS SAMs has been supported by observations that both of the SR_1 and SR_2 moieties constituting the initial R_1SSR_2 molecule are generally found in the same proportion in the resulting SAMs [60–63]. Note, as for AT SAMs, both thiolate-type surface bonding via S–S cleavage (analogous to S–H cleavage for AT) [61, 63], and the retention of disulphide bond upon adsorption was considered for SAMs formed from DDS [62].

During the characterization of different thiol-derived SAMs we found numerous evidences that these systems represent highly correlated molecular assemblies [50, 51]. Although most of these effects are not fully understood at present we describe and consider some of them in section 5.

2. Experimental procedure

The substrates were prepared by evaporation of 100–300 nm of gold or silver on mica (annealed after the evaporation) or titanium-primed (5 nm) polished single crystal Si(100) wafers [50]. These films predominantly exhibit a (111) orientation as e.g. concluded from the characteristic forward-scattering maxima in the angular distributions of the Au 4f and Ag 3d photoelectrons [64]. The SAMs were formed by 24 hours immersion of the substrates in 1 mmol solution of the corresponding substances in ethanol or dichlormethane [65] and subsequent rinsing. No contaminations or surface oxidation were detected.

All films were characterized by NEXAFS spectroscopy and XPS with a Mg Kα x-ray source. More detailed and complementary information was obtained by using synchrotron-based HRXPS. Additionally, IRRAS, contact angle measurements, and atomic force microscopy were applied to some of the systems. All experiments were performed at room temperature.

The NEXAFS experiments and the major part of the XPS measurements were carried out

in a home-made UHV chamber equipped with a VG CLAM 2 spectrometer. This chamber was attached to the HE-TGM 2 beamline [66] at the German synchrotron facility BESSY-1 in Berlin. The HRXPS measurements were performed at the synchrotron storage ring MAX II at MAX-Lab in Lund, Sweden, using the D1011 and I311 beamlines. Both beamlines are equipped with a Zeiss SX-700 plane-grating monochromator and a two-chamber UHV experimental station with a SCIENTA analyser.

The NEXAFS spectra were acquired at the C 1s absorption edge in the partial-yield mode with a retarding voltage of −150 V. The energy resolution was ∼0.65 eV. The incidence angle of the linear polarized light was varied from 90° to 20° to monitor the orientational order within the AT films. The raw spectra were normalized to the incident photon flux [31, 36, 67]. The energy scale was referenced to the π^*-resonance of highly oriented pyrolytic graphite at 285.38 eV [68]. The accuracy of the molecular tilt angles derived from the linear dichroism of the NEXAFS resonances was about 5°.

The XPS measurements with the Mg Kα x-ray source (1254 eV) were performed in normal emission geometry. The energy resolution was ∼0.9 eV. The energy scale was referenced to the Au $4f_{7/2}$ peak at 84.0 eV [69]. Both wide scan spectrum and the spectra for the C 1s, O 1s, F 1s, S 2p, and Au 4f (or Ag 3d) regions were measured for each sample. As a rule, the spectra were normalized to the total electron yield to correct for small differences in sample positions and x-ray source intensities [31, 36, 67]. From the XPS data the film thicknesses were derived using the intensity ratios of the C 1s and Au4f/Ag4d emissions [33, 70] and the intensity ratios of the Au4f/Ag4d emission for the film-covered and clean gold/silver substrate [58]. The attenuation lengths of the C 1s, S 2p, Au 4f, and Ag 3d photoelectrons were taken as ∼27 Å, 28.5 Å, 30–31 Å, and 26 Å, respectively [33, 70].

For the HRXPS measurements excitation energies in the range of 140–580 eV were used. For the probed S 2p, C 1s, Au 4f, and Ag 3d core levels a tremendous increase of the photoionization cross-sections occurred at these excitation energies as compared to the respective values for the Mg Kα x-ray source [71, 72]. The energy resolution was better than 0.1 eV, which is noticeably smaller than the full widths at half maximum (FWHMs) of the photoemission peaks of this study. Thus, the acquired HRXPS spectra reflected the intrinsic energy spread of the core-level photoemission process. The high energy resolution required special care for the energy calibration: this procedure was performed individually for every spectrum. The energy scale was referenced to the pronounced Au $4f_{7/2}$ 'bulk' peak (83.93 eV) of a reference C12/Au sample, which was attached to the same sample holder as the probed sample. A value of 83.93 eV was derived from independent calibrations to the Fermi edge of a clean Pt-foil, which is very close to the value of 84.0 eV used as the reference for the XPS measurements with a Mg Kα x-ray source.

The HRXPS and XPS spectra were fitted using Doniach–Sunjic peak profiles and a Shirley type or a parabolic background. To fit the S $2p_{3/2,1/2}$ doublet we used two peaks with the same FWHM, the standard spin-orbit splitting of ∼1.2 eV (verified by fit), and the branching ratio of 2:1 ($S2p_{3/2}$/$S2p_{1/2}$).

Infrared adsorption measurements were performed with a dry-air-purged Bio-Rad FTIR spectrometer Model FTS 175C equipped with a liquid nitrogen cooled MCT detector. All spectra were taken with p-polarized light with a PIKE advanced grazing angle accessory at a fixed incident angle of 80° with respect to the surface normal. The measurements were carried out in the range of 650–4000 cm^{-1} at a resolution of 2 cm^{-1} and with at least 1000 scans per spectrum. The spectra are given in absorbance units $A = -\log R/R_o$, where R and R_o are the reflectivities of the sample and reference, respectively. As a reference we used SAMs of perdeuterated n-eicosanethiols, whose C–D absorption bands at 2050–2200 cm^{-1} do not interfere with the spectral region of interest [70].

3. Balance of structural forces in thiol-derived SAMs

3.1. Aliphatic SAMs

To reveal the role of the headgroup–substrate interaction in aliphatic thiol-derived SAMs we varied the strength and character of the chain–chain interaction by substituting the terminal methyl group of the AT by a perfluoro nonane [30, 31] or methylated BP moiety [30, 32, 51] and studied the F10Hn ($n = 11, 17$) and BPn SAMs ($n = 3$–6) on gold and silver substrates (also F10H2 films have been characterized [31]). As expected, these SAMs were found to consist of intact F10Hn or BPn molecules bonded to the substrate via the sulphur headgroup [31, 32].

In SFAT SAMs, the attachment of the bulky fluorocarbon chain with a vdW diameter of 5.6 Å as compared to 4.2 Å for the hydrocarbon chain [23] leads to an increase in lateral spacing for the hydrocarbon moieties [73–76], which consequently results in a significant (by a factor of 2–3 as compared to AT SAMs [19]) reduction of the intermolecular vdW interaction between the alkyl chains. Assuming that the interchain vdW interaction is an essential factor in determining the difference in orientation of the AT molecules in AT SAMs on Au and Ag, the disappearance of this difference is expected for the hydrocarbon parts of the SFAT molecules separated farther than the equilibrium vdW spacing. Note, that SFAT SAMs (as well as SAMs formed from alkyl fluoroalkyl disulphides and semifluorinated amidethiols [60, 62, 77]) have been previously studied on gold substrates only [73–78]. No data for silver substrates are available.

The larger vdW diameter of the fluorocarbon chains in SFAT SAMs is mainly due to their helical conformation, which is typical for long-chain perfluoroalkanes. The IR spectra in the CF-stretching region (figure 1) show adsorption bands at 1375 cm^{-1}, 1346 cm^{-1}, and 901 cm^{-1} suggesting that the helical conformation is retained in the SFAT films on both the Au and Ag substrates [73, 77, 78]. The hydrocarbon moieties in the adsorbed SFATs have a planar zigzag conformation as in conventional AT SAMs, which was confirmed by the characteristic asymmetric and symmetric methylene stretching modes [25, 79] at $\nu_a(CH_2) = 2919$ cm^{-1} and $\nu_s(CH_2) = 2851$ cm^{-1} in the IR spectra in the CH-stretching region (figure 2). A larger integral intensity of the C–H stretching vibrational modes (the transition dipole moments of these modes are perpendicular to the molecular axis) on gold as compared to silver means that the hydrocarbon chains in SFAT SAMs on gold are more strongly canted. The twist angle of these chains, which defines the rotation of the alkyl carbon backbone about the chain axis with respect to the plane defined by this axis and the surface normal, can be calculated from the intensity ratio of the asymmetric and symmetric C–H stretching modes following the RATIO method by Debe [80]. This approach resulted in twist angles of $54^\circ \pm 3^\circ$ and $58^\circ \pm 3^\circ$ for F10H11/Au and F10H17/Au and $48^\circ \pm 3^\circ$ and $47^\circ \pm 3^\circ$ for F10H11/Ag and F10H17/Ag, respectively, which, within the errors, are identical to the respective values of 53° and 45° found for conventional AT SAMs on these substrates [21].

The IR results are supported by the NEXAFS data. The predominant features of the NEXAFS spectra (figure 3) are the resonances at ∼292 eV, ∼295 eV, and ∼299 eV which are related to the transitions from the C_{1s} state to the C–F σ^*, C–C σ^*, and C-F′ σ^* orbitals of the fluorocarbon part, respectively [77, 81, 82]. The corresponding transition dipole moments are oriented almost perpendicular ($C_{1s} \rightarrow$ C–F σ^*) and along the chain axis ($C_{1s} \rightarrow$ C–C σ^*) [77, 81–83]. From the hydrocarbon part, only a small resonance at ∼288 eV commonly assigned to the C_{1s} excitations into pure valence C–H orbitals [84], predominately Rydberg states [85, 86] or mixed valence/Rydberg states [87] is observed (we denote this resonance as an R^* resonance). The orbitals related to the R^* resonance are oriented perpendicular to the alkyl

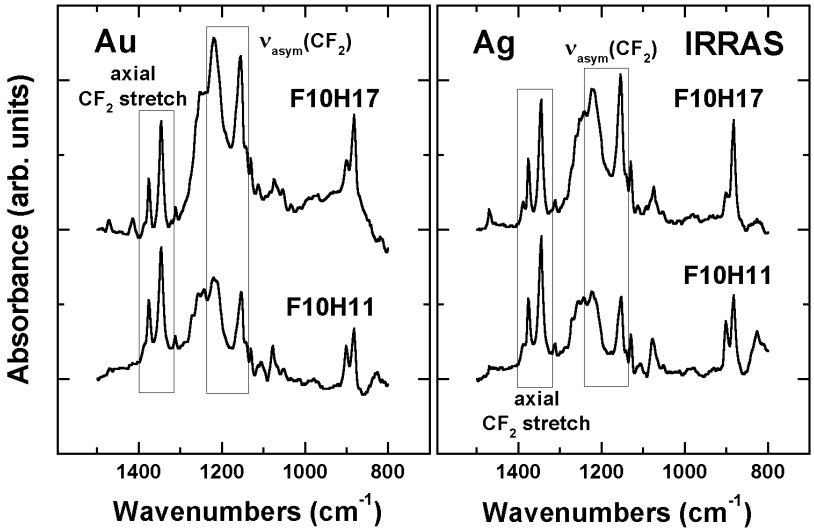

Figure 1. IR absorption spectra in the CF-stretching region for the SFAT films on gold and silver. The vertical scale in the left and right panels are the same.

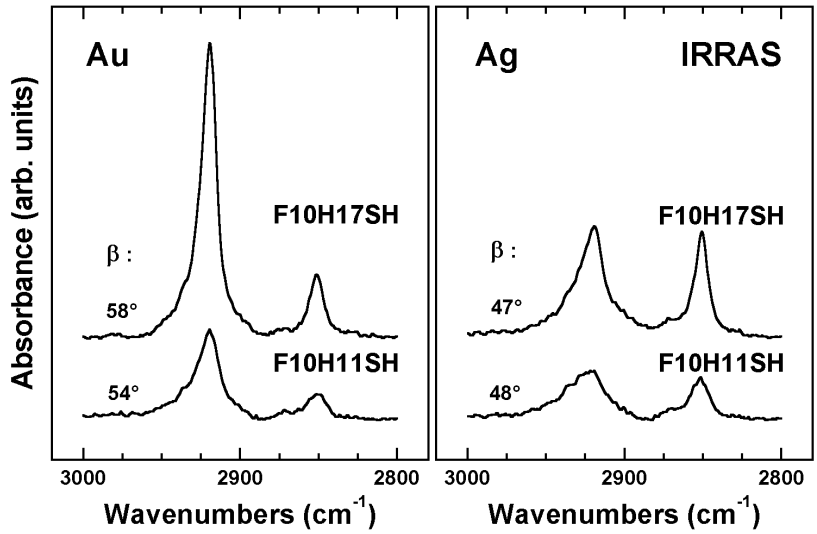

Figure 2. IR absorption spectra in the CH-stretching region for the SFAT films on gold and silver. The vertical scale in the left and right panels are the same. The derived twist angles of the hydrocarbon chains β are displayed at the respective spectra.

chain axis [26, 83, 88]. The positions of the NEXAFS resonances related to the fluorocarbon entities and the spectral shape are very similar to the calculated NEXAFS spectra for bulk poly(tetrafluoroethylene) assuming the standard [89] 13/6 or 15/7 helix for the fluorocarbon chains [90].

The pronounced linear dichroism of the NEXAFS spectra, i.e. their dependence on the angle of light incidence, implies well-ordered and densely packed layers [84] (no orientational

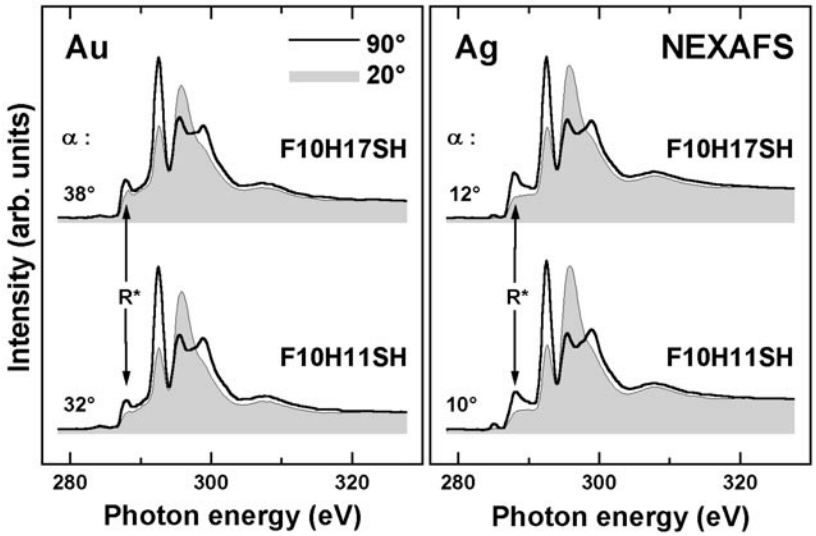

Figure 3. C 1s NEXAFS spectra of F10H11 and F10H17 on Au and Ag at normal (90°) and grazing (20°) x-ray incidence. The grazing incidence spectra are shadowed. The derived average tilt angles of the hydrocarbon chains α are displayed at the respective spectra.

order can be expected in loosely packed films). The average tilt angles of the fluoro- and hydrocarbon chains in these layers were determined from the angular dependence of the C–F σ^* and R* resonance intensities, respectively (figure 4) [84, 88]. For the fluorocarbon chains similar values are obtained on gold and silver [31], but a significant substrate dependence of the tilt angles is obtained for the hydrocarbon moieties, in full agreement with the IR data. On Au, the hydrocarbon chains are inclined by 32–38° with respect to the surface normal and on Ag they are canted by 10–12°. Thus, the hydrocarbon parts of the SFAT films practically exhibit the same correlation between the tilt and twist angles and the substrate metal as hydrocarbon chains in conventional AT SAMs.

Let us now turn to the BPn SAMs. In these films the attachment of the methylated BP tail groups to the relatively short alkanethiol chains changes the character and strength of the intermolecular interaction. Unless the sulphur–substrate bond plays a decisive role, one expects that the relatively strong interaction between the rigid BP moieties determines the structure of the BPn SAMs independently of the length of the alkane chains and the substrate.

The respective C 1s NEXAFS spectra are depicted in figure 5, while the normalized XP C 1s spectra along with the derived C1s/Au4f and C1s/Ag3d integral intensity ratios are presented in figure 6. The dominant feature in the NEXAFS spectra in figure 5 is the π_1^* resonance at 285.1 eV related to the aromatic rings in the BP moieties and having a transition dipole moment perpendicular to the ring plane. The observed linear dichroism of this resonance suggests well-ordered films with an average tilt angle of the BP moieties depending both on the number of CH_2 units in the alkyl chain and on the substrate. On the basis of this linear dichroism, a value of the average tilt angles of the BP moieties in the BPn SAMs was obtained [84] assuming a herringbone arrangement [9, 10, 12] and planar conformation [12, 34, 93] of these moieties. Such an arrangement suggests two different spatial orientations of the BP moieties with the same tilt angle with respect to the surface normal but reverse twist angles with respect to the plane defined by the surface normal and the moiety axis. Regardless of the twist angle and its variation with the length of the aliphatic part there is a significant change in

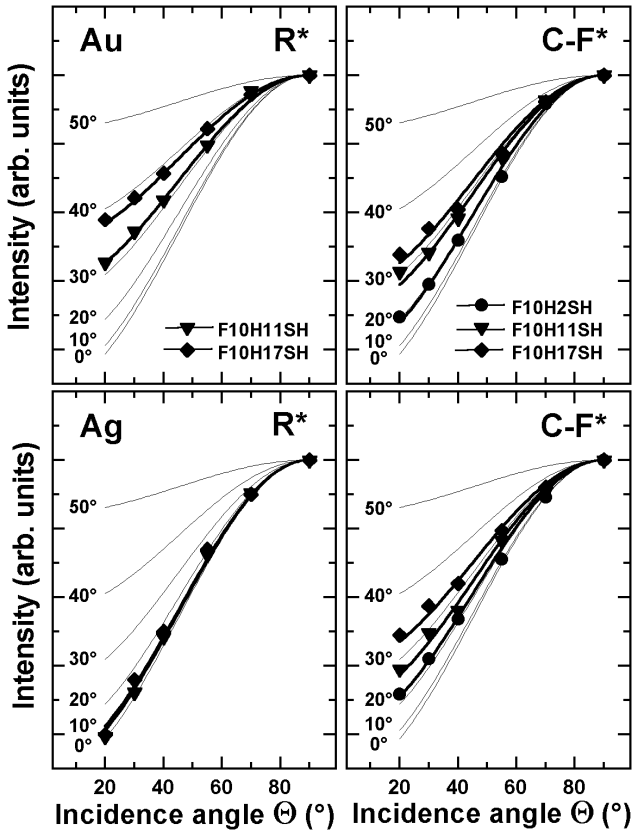

Figure 4. The angular dependences of the R*- and C–F σ^*-resonance intensity for F10H2 (circles), F10H11 (triangles) and F10H17 (diamonds) on gold and silver. Also the theoretical dependencies (thin solid lines) for different tilt angles of the hydrocarbon and fluorocarbon chains are presented. The perpendicular orientation of the C–F σ^*-orbital with respect to the fluorocarbon chain axis is assumed. The derived tilt angles of this chain should be, therefore, corrected for a slight tilt of the CF_2 planes toward the helix axis [30].

the tilt angle of the BP units, this effect being inverse for the Au and Ag substrates (the derived tilt angles are displayed at the respective spectra in figure 5) [32]. Thus, the bulky BP moiety reveals orientation changes analogous to the behaviour of the methyl end group of n-alkane thiols on Au and Ag [21, 28, 29].

However, there is an important difference between SAMs consisting of BPn and *n*-alkane thiols. In contrast to *n*-alkane thiols which do not exhibit a chain length dependence of coverage [21, 28], the molecular density in the BPn layers alternates with the number of methylene groups in the alkyl part as seen from the respective dependences of the C1s/Au4f and C1s/Ag3d intensity ratios in figure 6. Again, there is an inversion of the alternating density between the Au and Ag substrates. The intensity changes correlate with the tilt angles of the BP moieties derived from the NEXAFS data: A more upright orientation of the aromatic unit allows for a higher packing density. On Ag, the odd-even effect of the packing density also manifests itself in the position of the C1s XP peak (see also HRXPS spectra in [51]). An even number of CH_2 (higher packing density) corresponds to an upward shift of the C1s binding energy.

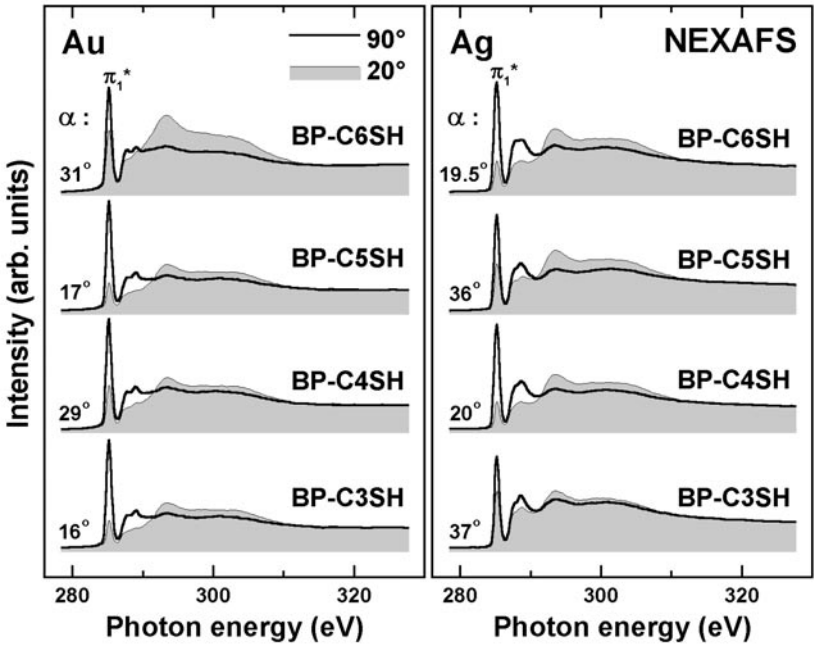

Figure 5. C 1s NEXAFS spectra for SAMs formed from BPn ($n = 3$–6) on gold and silver substrates at normal (90°) and grazing (20°) x-ray incidence. The derived average tilt angles of the BP moieties α are displayed at the respective spectra. These angles were obtained assuming a herringbone arrangement of the BP moieties with a twist angle as found for the respective bulk systems [91, 92].

The above results can only be explained by assuming that the hybridization and thus spatial orientation of the binding orbitals of sulphur is a determining factor for the orientation of the alkyl chains and consequently for the structure of SFAT and BPn SAMs. Comparing SFAT and AT SAMs on the same substrate (Au or Ag) one finds almost the same orientation of the hydrocarbon moieties despite the difference in the chain–chain interaction determined by the intermolecular separation. The common structure determining factor between these two systems is the sulphur–substrate interaction. A change in this interaction at going from the Au to Ag substrate results in the same change of the molecular orientation in both the AT and SFAT SAMs. In BPn films the orientation and the packing density of the rigid and strongly interacting BP moieties is influenced by the orientation of the adjacent CH_2–CH_2 segment, whose orientation is a function of the number of CH_2 units in the alkyl chain and the surface–S–C bond angle. For all-trans alkyl chains with C–C–C bond angles of $\sim$112° and the surface–S–C angles tending to ideal values of $\sim$104° (Au) and $\sim$180° (Ag) [1, 29, 94], a more tilted orientation of this segment is expected for an odd number of methylene units in the alkyl part of BPn/Au and an even number of these units in BPn/Ag (see [32] for details). This orientation allows for a more upright orientation of the adjacent BP moieties (a smaller tilt angle), and consequently a denser molecular packing. Similarly, for an even number of the CH_2 units in the BPn SAMs on Au, and for an odd number of these entities for BPn on Ag, a less tilted orientation of the BP-adjacent CH_2–CH_2 segment of the alkane chain is expected resulting in a larger tilt of the adjacent BP moieties and thus a reduced density. Note, that although there is a significant driving force to pertain a sp^3 and a sp bonding configurations of the sulphur headgroups on gold and silver, respectively, the pronounced odd-even changes

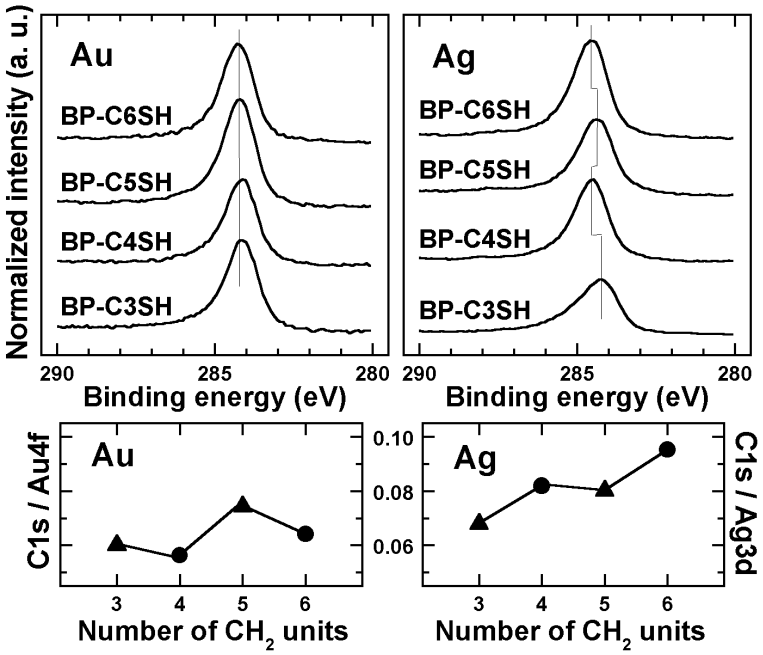

Figure 6. Normalized C 1s XPS spectra for SAMs formed from BPn ($n = 3$–6) on gold and silver substrates together with the derived C1s/Au4f and C1s/Ag3d integral intensity ratios.

in the molecular orientation and the packing density of the BP moieties affect to some extent the character and geometry of the headgroup–substrate bonding. The S 2p HRXPS spectra of the BPn SAMs (figure 7) exhibit odd-even variation of BE, FWHM, and the total intensity of the S $2p_{3/2,1/2}$ peaks (figure 8). Whereas the BE changes are presumably related to the small variation in the character of the headgroup–substrate bond, and the intensity changes stem from the variation of the packing density and thickness of the BPn films, the FWHM changes are associated with the occupation of either equivalent or non-equivalent adsorption sites on the polycrystalline (111) Au and Ag substrates (see next section and [51] for details).

In general, the results for the SFAT and BPn SAMs imply that the headgroup–substrate interaction is a decisive factor in the structure of the thiol-derived aliphatic SAMs on gold and silver substrates. Further support for this conclusion are AT SAMs on gold exposed to mercury vapour, as recently reported by Thome *et al* [33]. Such an exposure results in the penetration of mercury atoms through the AT film and their adsorption/intermixing on/with the gold so that a mercury bulk concentration of 14–16 atomic% is achieved in the vicinity of the Au substrate surface. We have monitored the structural changes in the AT film by NEXAFS spectroscopy [33]. The NEXAFS spectra at normal (90°) and grazing (20°) x-ray incidence for C16 SAMs on gold before and after exposure to mercury vapour, as well as after subsequent reimmersion in C16 solution are depicted in figure 9.

The most pronounced spectral features in figure 9 are a sharp R* resonance at ∼287.7 eV (see above) and the broader C–C and C–C′ σ^* resonances at 293.4 eV and 302 eV, respectively [83–85]. Whereas the molecular orbitals related to the R* resonance are oriented perpendicular to the molecular axis of the alkyl chains, the transition dipole moments of the molecular orbitals corresponding to the σ^* resonances are believed to be directed along the alkyl chain axis [83]. In agreement with this assignment, the R* and C–C–/C–C′ σ^*-resonances change their intensities

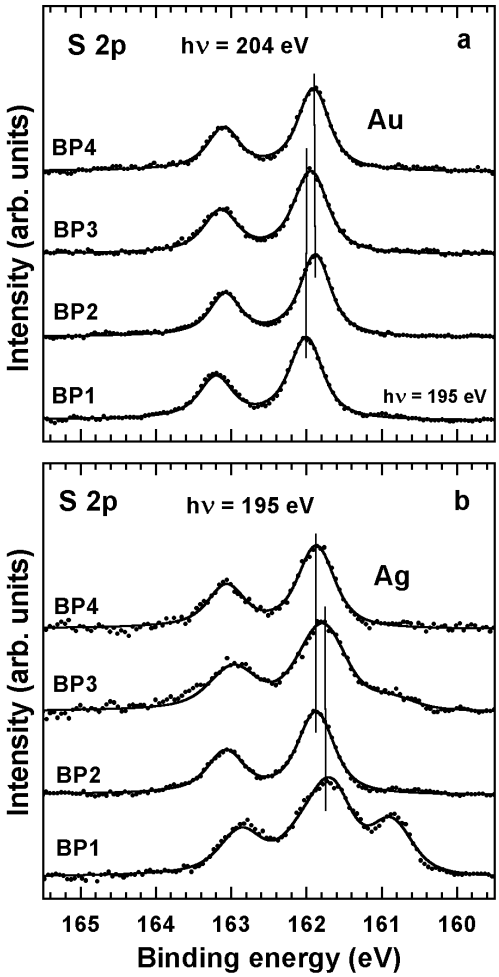

Figure 7. S 2p HRXPS spectra for BPn SAMs on Au and Ag. The positions of the S $2p_{3/2}$ peak are marked by thin solid lines. There is an additional sulphur species in BP1/Ag. The spectra are normalized to the same amplitude of the S $2p_{3/2}$ peak.

in the opposite way at going from the normal to grazing incidence spectra. The observed linear dichroism implies well-ordered alkanethiol layers.

The spectra for the C16 film exposed to Hg exhibit, however, a larger linear dichroism than those for the pristine film. Moreover, a further increase of the linear dichroism is observed in the spectra of the mercury-processed film after the reimmersion in the thiol solution. Quantitative analysis yields average tilt angles of the AT chains of $\sim 35^\circ$ $\sim 26^\circ$, and 23° for the untreated, mercury exposed, and thiol-solution-reimmersed C16 sample, respectively [33]. These values imply a decrease of the tilt angle by $\sim 9^\circ$ after exposure to mercury vapour and by $\sim 12^\circ$ after this exposure and subsequent reimmersion in the thiol solution.

The drastic decrease of the AT chain tilt angle after exposure of C16/Au to mercury vapour can be only related to the gold substrate modification through the adsorption of Hg and its presumable intermixing with gold. A decisive influence of the headgroup–substrate interaction on the entire structure of the AT SAMs is, thus, obvious. The reorientation of the

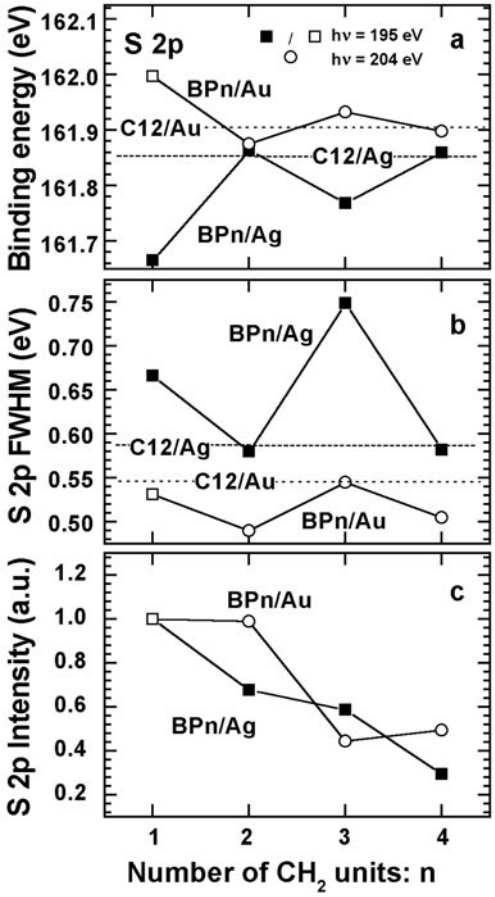

Figure 8. BE (a) and FWHM (b) of the S $2p_{3/2,1/2}$ peaks derived from the S 2p spectra in figure 7 as well as the normalized intensity of the S 2p doublet (c). The respective values for AT SAMs are given as dashed lines in (a) and (b). The accuracy of the BE and FWHM values is ±0.01 eV.

AT chains occurs even in spite of the energetically unfavourable agglomeration of initially almost homogeneous AT layer in domains. The formation of such domains is the single way to decrease the tilt angle, because a smaller tilt angle corresponds a larger packing density and there is only a limited number of molecules in the untreated C16 SAM.

There is also a direct evidence of AT chain agglomeration after exposure of C16/Au to mercury, namely a pronounced increase of the entire C 1s XPS signal after reimmersion of the mercury-processed C16 film in the thiol solution [33]. During this reimmersion the AT film accumulates a necessary amount of the AT chains in the holes at domain boundaries and/or in less closely packed domains to get a homogeneous, closed AT layer on the Hg/Au surface. This procedure results in the increase of the orientational order in the AT film as seen in figure 9. As a fingerprint of this process, the average tilt angle of the alkyl chain increases by $\sim 3^\circ$. This increase can be related to the reorientation of initially poorly oriented AT chains at domain boundaries due to the intermolecular interaction with the newly incorporated AT entities.

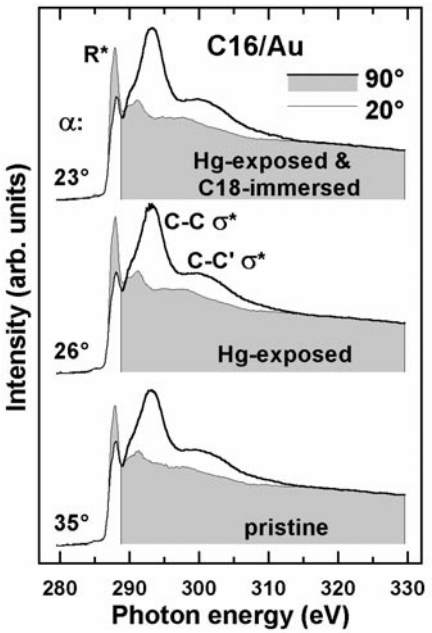

Figure 9. C 1s NEXAFS spectra of C16 SAM on Au acquired at normal (90°) and grazing (20°) x-ray incidence. The grazing incidence spectra are shadowed. Bottom, pristine film; middle, after exposure to mercury vapour; top, after reimmersion in the thiol solution. The derived average tilt angles of the aliphatic chains α are displayed at the respective spectra.

3.2. Aromatic SAMs

As mentioned in section 1, the balance between the intermolecular and headgroup–substrate interactions in the thioaromatic films can be somewhat different as compared to the thioaliphatic SAMs.

In agreement with expectations, the investigated TP, BPT, TPT and AnT SAMs were found to consist of the intact molecules bonded to the substrate via the sulphur headgroup. A single S $2p_{3/2}$/S $2p_{1/2}$ doublet at approximately the same BE of ∼162.0 eV (S $2p_{3/2}$) was observed in the respective XPS spectra for both substrates (figures 10(c) and (d)), while a single C 1s photoemission maximum at a BE of ∼284.5 eV with a higher BE tail were exhibited in the C 1s XPS spectra, except for TP/Au, where several additional peaks can be distinguished (figures 10(a) and (b)). With the same exception, the intensities of the S $2p_{3/2}$/S $2p_{1/2}$ doublets for both substrates reveal the expected reduction by going from TP to BPT and further to TPT, which is related to the increasing attenuation of the S 2p photoelectrons by the thicker aromatic overlayer. In the same manner as the S 2p emissions, the integral intensities of the C 1s features correlate with the molecular compositions of the respective SAMs. As to AnT, a less dense packing of the AnT molecules is suggested for AnT/Au as compared to AnT/Ag, based on the S 2p and C 1s XPS spectra in figure 10. Note, that the S 2p and C 1s intensities for the AnT SAMs should be presumably closer to those for the BPT films (as found on Ag) considering that the rigid AnT molecules with an off-axis thiol group need somewhat more space than the flexible BPT or TPT molecules, and that the AnT molecule has two carbon atoms more and four less than BPT and TPT, respectively.

The C 1s NEXAFS spectra of the TP, BPT, TPT, and AnT SAMs on Au and Ag acquired at the magic angle of x-ray incidence (55°) are depicted in figure 11. The spectra acquired at

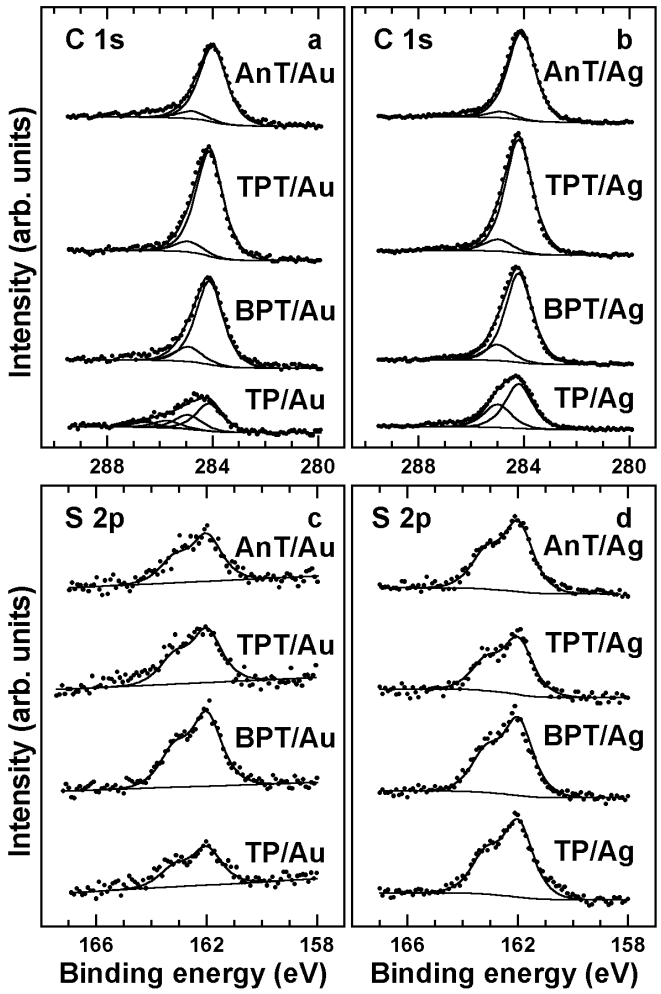

Figure 10. The normalized C 1s ((a) and (b)) and S 2p ((c) and (d)) XPS spectra of the TP, BPT, TPT and AnT monolayers on Au ((a) and (c)) and Ag ((b) and (d)) surfaces. The measurements were performed with the Mg Kα x-ray source (1254 eV) in normal emission geometry.

this geometry exclusively reflect the electronic structure of the unoccupied molecular orbitals of the investigated films and are not affected by the angular dependence of the adsorption cross-sections [84]. The spectra in figure 11 exhibit a C 1s absorption edge related to C $1s \rightarrow$ continuum excitations located at $\approx$287 eV [6, 12] and several pronounced π^* and σ^* resonances. The spectra of the TP, BPT and TPT monolayers are quite similar because of localization of the π^* orbitals by the creation of a C1s core hole [95, 96], whereas the spectrum of the AnT film reveals a more complex π^* resonance structure related to the chemical shift of the two symmetry independent carbon atoms mediated by excitonic effects [97, 98]. Similar to benzene [99, 100] and TP on Mo(110) [84, 101, 102], the spectra of TP, BPT and TPT films are dominated by a strong π_1^* resonance at 285.0 eV, accompanied by a weaker π_2^* resonance at 288.9 eV. The spectra of the AnT films exhibit a pronounced splitting of the π_1^* resonance into the π_{1a}^* and π_{1b}^* resonances at 284.4 eV and 285.7 eV [95, 97].

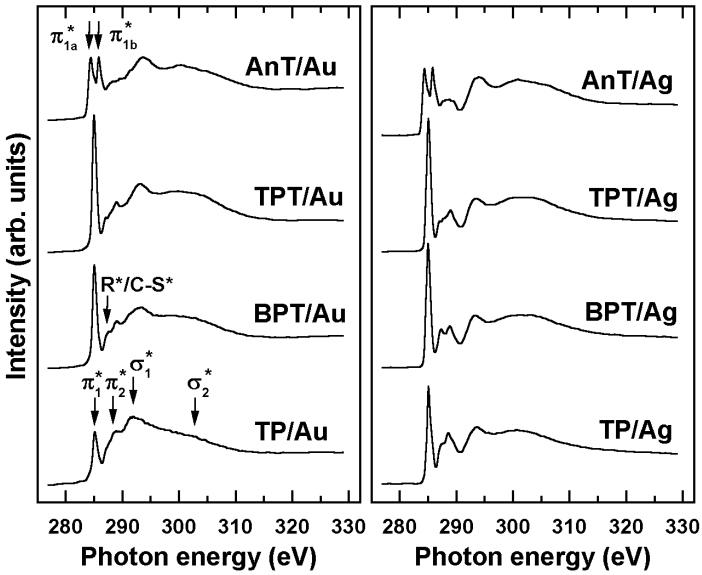

Figure 11. The C 1s NEXAFS spectra of TP, BPT, TPT, and AnT on Au and Ag acquired at the magic angle of x-ray incidence (55°). The characteristic absorption resonances are indicated by arrows.

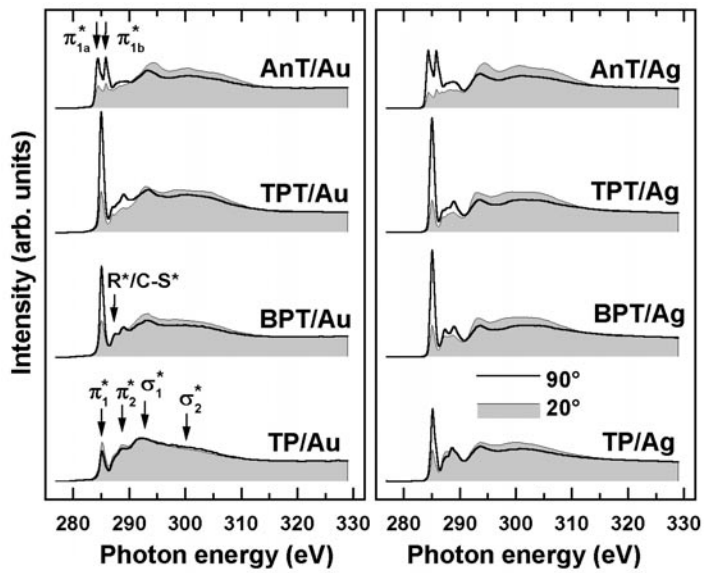

Figure 12. The C 1s NEXAFS spectra of TP, BPT, TPT, and AnT on Au and Ag acquired at normal (90°) and grazing (20°) x-ray incidence. The grazing incidence spectra are shadowed. The characteristic absorption resonances are indicated by arrows.

The NEXAFS spectra for all investigated SAMs (except for TP/Au) exhibit an increase of the π^* resonance and a decrease of the σ^* resonance intensity with increasing angle of the light incidence (see figure 12), which implies an upright orientation of the thioaromatic molecules

in the respective SAMs. The reverse behaviour of the σ^* and π^* resonance intensities is related to the orthogonal orientation of the π^* and σ^* orbitals. In the case of TP/Au, the decrease of the π^* resonance intensity suggests a preferential orientation of the phenyl rings parallel to the substrate surface.

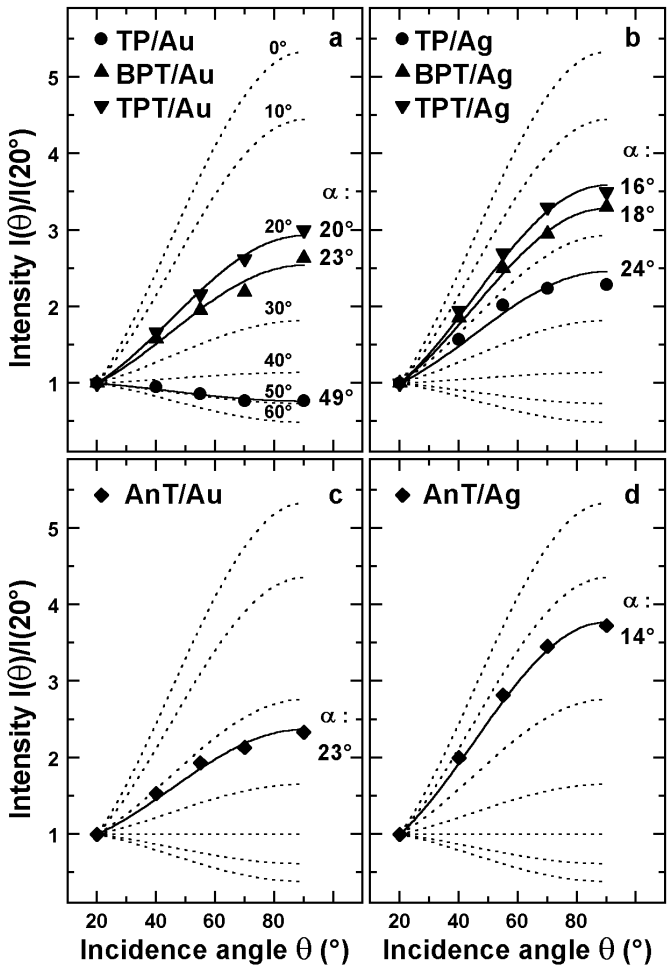

Figure 13. The angular dependencies of the π_1^* intensity ratios for TP (circles), BPT (up triangles), TPT (down triangles) and AnT (diamonds) adsorbed on Au and Ag surfaces. For comparison, the theoretical dependencies for different tilt angles of the aromatic backbone are added as dotted lines. The derived average tilt angles of the aromatic chains α are displayed at the respective fitting curves.

On the basis of the linear dichroism of the most intense π_1^*/π_{1a}^* resonance [84] a value of the average tilt angle of the thioaromatic molecules in the respective SAMs was obtained. A herringbone arrangement [9, 10, 12] and planar conformation [12, 34, 93] of the thioaromatic molecules was assumed as for the BP moieties in the BPn SAMs (see previous section). However, for the absolute intensities, we used instead the intensity ratios $R = I(\theta, \beta, \alpha)/I(20^\circ, \beta, \alpha)$ (figure 13) and assumed the same twist angles β of 32° for the TP, BPT and TPT films and 26° for the AnT SAMs as found for the respective bulk systems [91, 92, 103, 104]. This assumption is supported by the analysis of the calculated 2D molecular

arrangements for BP and naphthalene on Au [9] and by the experimental data for a series of oligo(phenylethynyl)benzenethiols [10] and BPn films [32]. The determined average tilt angles α for TP, BPT, TPT and AnT SAMs are 49°, 23°, 20°, and 23° in the case of the Au substrate and 24°, 18°, 16°, and 14° in the case of the Ag substrate. The film thicknesses obtained based on these tilt angles correlate well with the respective values derived from the analysis of the XPS spectra [36]. The average tilt angle for BPT/Au coincides within the error bars with the respective value from a recent x-ray diffraction study [17], where a tilt angle of 19° was found for 4-methyl-4′-mercaptobiphenyl layers on Au(111).

Whereas TP/Au seems to be a poorly defined film with a random molecular orientation, all other films are well ordered. Similar to the AT chains in AT SAMs, thioaromatic molecules exhibit smaller tilt angles with respect to the surface normal on Ag as compared to Au substrates. However, the absolute difference of the tilt angles on Au and Ag is smaller than that for the alkanethiols. Excluding the relatively short TP, the thioaromatic SAMs reveal an average tilt angle of ≈22° on Au and ≈16° on Ag compared to the long chain alkanethiols with average tilt angles of ≈30° and ≈12°, respectively. We assume that the difference between the thioaromatic and aliphatic films is related to a stronger influence of the intermolecular interaction in the former systems, so that the respective forces become a major structure-determining factor. An additional support for this assumption is that in contrast to the chain length independent tilt angle of long chain alkanethiols, the tilt angle of aromatic molecules in the respective SAMs varies slightly with the length of the aromatic chain on both Au and Ag substrates. Even the rigidity of the thioaromatic molecule affects the final molecular orientation within the layer to a smaller extent than the number of aromatic moieties, as follows from the comparison of the results for AnT and BPT/TPT films.

Nevertheless, the substrate is still a decisive factor for the structure of the thioaromatic films. First, despite the strong intermolecular forces there still is a difference in the average tilt angles on Au and Ag substrates. Second, for the TP monolayers on Au and Ag the effect of the substrate on the SAM structure is crucial: the poor quality of the TP monolayers on Au can probably be explained by steric constraints caused by the pinning of the TP molecules to a definite adsorption site because of the large corrugation of the sulphur–metal BE surface [1, 18].

Note that in contrast to the AT SAMs, the substrate–S–phenyl bond angle, which is associated with a definite hybridization of the S-atom (see section 3.1) can be rather similar in the thioaromatic films on both substrates. Along with the enhanced intermolecular interaction, this similarity can be an additional factor responsible for the relatively small differences observed in the tilt angles of the thioaromatic molecules on Au and Ag. Generally, the surface bonding of a S atom at a phenyl ring cannot be easily described by sp^3- or sp- hybridization, but is due to the aromatic ring associated with an intermediate state, which is not precisely known at present.

4. Chemical identity of the headgroup and absorption site homogeneity at the S-metal interface

Both the most intense Au 4f and Ag $3d_{5/2}$ XPS lines ascribed to the Au and Ag core levels and the S 2p emission related to the SAM headgroup were monitored to characterize the S–metal interface in the thiol-derived SAMs. The Au 4f and Ag $3d_{5/2}$ spectra of the clean and AT/BPT-covered gold and silver substrates are presented in figures 14 and 15, respectively. The Au $4f_{7/2,5/2}$ emission of the clean gold substrate exhibits two components (83.93 eV and 83.62 eV with a FWHM of 0.42 eV for $4f_{7/2}$), which can be assigned to the gold atoms in the bulk and topmost surface layer, respectively. This assignment is supported by the intensity

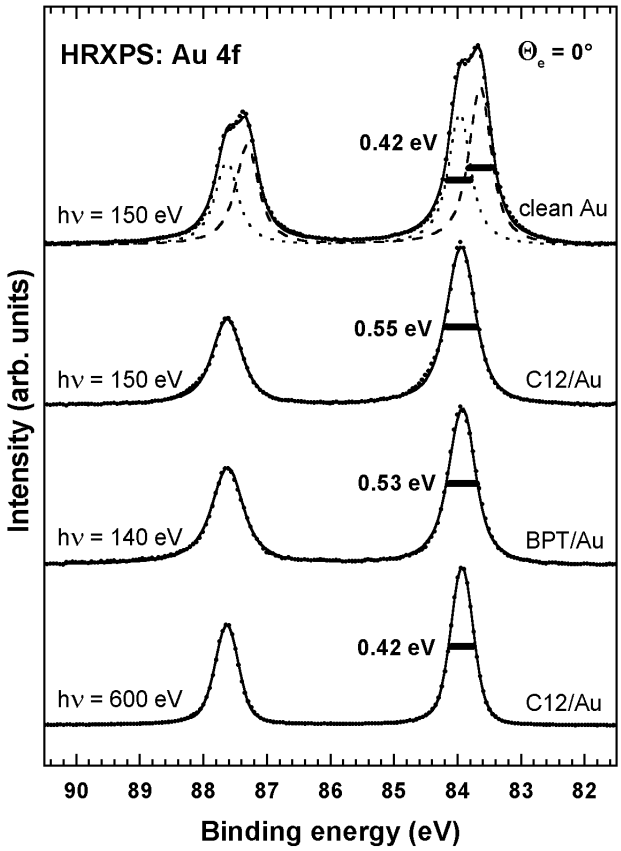

Figure 14. Au 4f HRXPS spectra of clean and C12/BPT covered gold substrate. For the spectrum of C12/Au the effect of the photon energy variation is demonstrated. The FWHMs of the Au $4f_{7/2,5/2}$ peaks are indicated. Θ_e is the take-off angle of the photoelectrons with respect to the surface normal.

increase of the surface component with increasing photoelectron take-off angle and by the good agreement of the observed surface core level shift of −0.31 eV with literature values [105–107]. Upon formation of both the AT or BPT SAMs a significant upward BE shift of the surface component occurs, resulting in spectra in which the bulk and surface (shifted by about −0.06 eV) components can only be derived by the peak fitting procedure assuming a constant BE position of the bulk component. The bulk emission can be emphasized by increasing the kinetic energy of the photoelectrons, which results in the decrease of the FWHM of the Au $4f_{7/2}$ peak for AT/Au from ∼0.55 eV to ∼0.42 eV (bottom spectrum in figure 14), the latter value is identical to the FWHM of the surface and bulk Au $4f_{7/2}$ components for the clean gold surface.

In the case of the clean silver surface only one Ag $3d_{5/2}$ peak with a BE of 368.25 eV and a FWHM of ∼0.37 eV is discernible in the respective XPS spectrum (figure 15), which is in agreement with literature data [106, 108] and implies that the BEs of the surface and bulk components for the Ag(111) surface are very close. From an analysis of the spectra with increasing photoelectron take-off angle (a FWHM of 0.39 eV at 40° and 0.43 eV at 70°) the BE shift of the surface component can be estimated to be about +0.05 ± 0.03 eV.

Upon formation of the C12 or BPT SAM broadening of the Ag $3d_{5/2}$ peak occurs

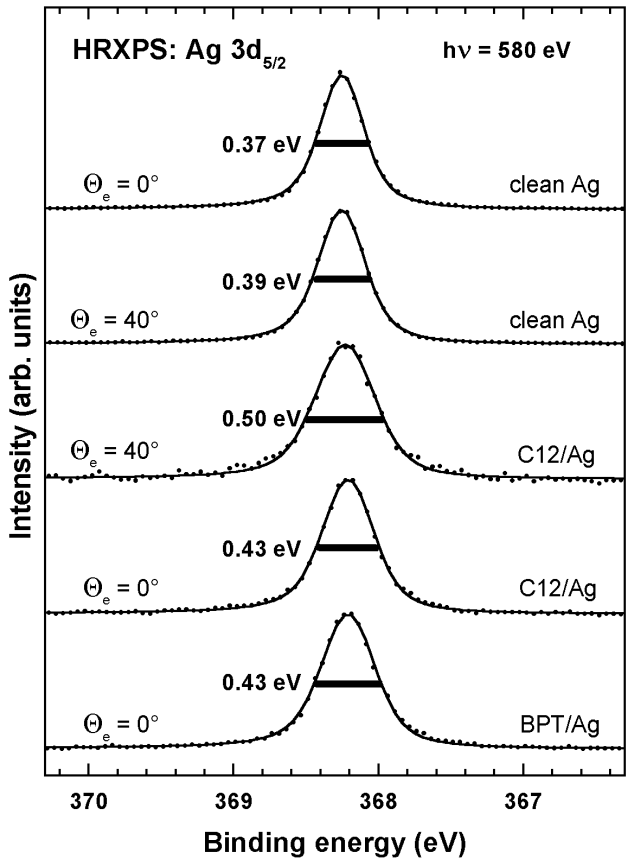

Figure 15. Ag $3d_{5/2}$ HRXPS spectra of clean and C12/BPT covered Ag substrate. The effect of the take-off angle variation is shown. The FWHMs of the Ag $3d_{5/2}$ peaks are indicated. Θ_e is the take-off angle of the photoelectrons with respect to the surface normal.

(figure 15). In particular, the FWHM of this peak for AT/Ag increases to 0.43 eV and 0.50 eV at take-off angles of 0° and 40°, respectively (for BPT/Ag very similar values were found). There is also a slight downward BE shift of the Ag $3d_{5/2}$ emission at larger take-off angles after SAM formation, e.g. a displacement by −0.06 eV at a take-off angle of 50°. A self-consistent fit of the Ag $3d_{5/2}$ spectra by two peaks of same FWHM gives a BE shift of the surface component of -0.11 ± 0.03 eV. Thus, whereas the BE differences of the Au 4f/Ag $3d_{5/2}$ bulk and surface components are distinctly different for the clean Au and Ag surfaces, similar BE differences are observed for both substrates after AT/BPT adsorption. The significant BE shift of the Au4f/Ag3d surface components with respect to their positions for the clean substrates stems presumably from the chemical shift due to the chemisorption of the AT and BPT molecules. Note, that the difference in the BE shifts of surface components for the clean Au and Ag substrates can be related to the differences in the electronic structure of the two metals and to the $(\sqrt{3} \times 23)$ surface reconstruction of the clean Au(111) surface [109] which is lifted upon SAM formation [110].

The S 2p spectra of the AT and BPT SAMs are presented in figure 16. All S 2p spectra exhibit only one S 2p doublet with a BE of ∼161.9 eV (S $2p_{3/2}$) and a FWHM of the individual S $2p_{3/2,1/2}$ peaks of 0.53–0.58 eV. The exceptionally large FWHM of 0.73 for BPT/Au is caused

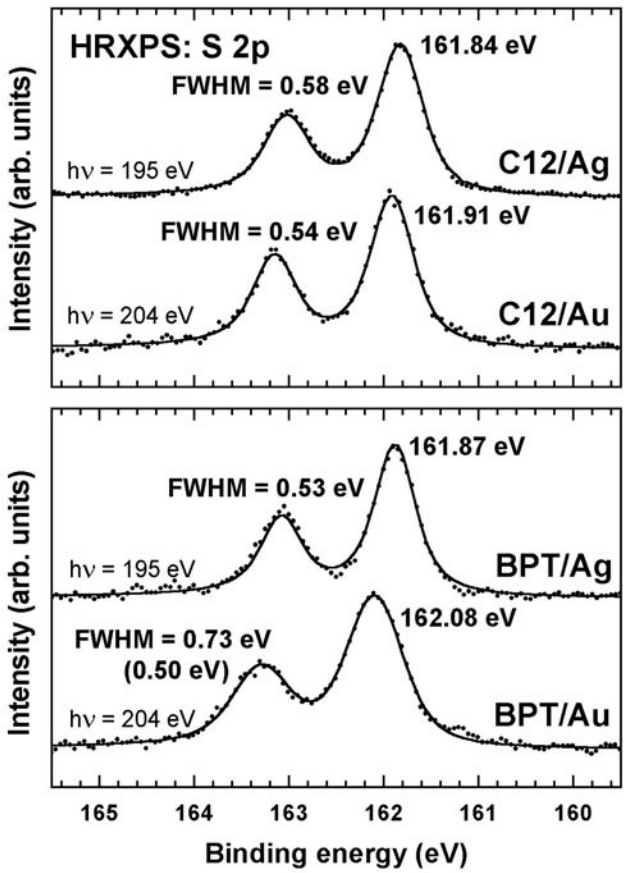

Figure 16. S 2p HRXPS spectra of AT and BPT SAMs on Au and Ag. The BEs and FWHMs of the S $2p_{3/2}$ peaks are indicated (see text for the FWHM of the S 2p peaks for BPT/Au).

by the limited quality of this particular sample: independent measurements performed by us on other BPT/Au and BPT/Ag samples at the SRRC in Taiwan gave a smaller (by ∼0.03 eV) FWHM of the S $2p_{3/2,1/2}$ peaks for BPT/Au as compared to that for BPT/Ag. Thus, the S $2p_{3/2,1/2}$ FWHM for a high quality BPT/Au should be ∼0.50 eV. Note that the difficulties in the reproducible fabrication of the latter films have been emphasized by other authors [17, 42].

The occurrence of only one S 2p doublet suggests that a single sulphur species is present in the AT and BPT SAMs on both substrates. Considering the conclusions of former XPS studies [21, 111] and the large BE difference with respect to unbound thiols (∼163.5 eV for S $2p_{3/2}$ [48, 112]) the single species found in our spectra is identified as a thiolate. The BE difference to unbound thiols stems from the chemical shift due to dissociation of the S–H bond and formation of a sulphur–metal bond and from screening of the S 2p core hole by the substrate electrons. The BEs of the S $2p_{3/2,1/2}$ peaks for the films on Ag are slightly smaller than those on Au, whereas the FWHMs of these peaks are slightly larger on Ag than on Au. While the BE difference for the two substrates may be related to a stronger S–substrate bonding on Ag [21, 28, 113, 114], the FWHM distinction can be associated with the generally assumed superposition of non-equivalent adsorption sites for the sulphur headgroups in AT/Ag and the equivalency of the adsorption sites in AT/Au (see section 1). For the latter system this equivalency is, however, not

absolute: the larger S $2p_{3/2,1/2}$ FWHM for AT/Au (0.54 eV) as compared to the corresponding values for BPT/Au (0.50 eV, as assumed) and for a loosely packed BPn/Au (0.50 eV, see figure 8) suggests slight differences in the adsorption geometry of the AT moieties in AT/Au. Considering the well-known c(4×2) modulation of the commensurate 2D lattice in AT/Au [27, 115–117] one can speculate about the existence of two different adsorption geometries. Taking into account a strong corrugation of the sulphur–Au binding energy hypersurface and the very small FWHM decrease (∼0.04 eV) by going from AT/Au to the BPT/Au or BPn/Au (even number of CH_2 units) this difference can be presumably assigned to slightly different adsorption heights or small lateral shifts of the sulphur atoms from equivalent high-symmetry adsorption sites. Different adsorption sites and largely different adsorption heights (as this i.e. was assumed in [46]) should presumably result in a noticeably larger increase of the FWHM of the S $2p_{3/2,1/2}$ peaks. Note, that a S $2p_{3/2,1/2}$ FWHM of 0.50 eV should be representative for the fully commensurate $(\sqrt{3} \times \sqrt{3})R30^\circ$ surface lattice, taking into account that such a lattice was found for the high-quality BPT film on Au(111) [17] and considering that a value of 0.50 eV is the smallest one observed for thiol-derived SAMs.

The above-described results imply an individual bonding of the AT chains to the Au and Ag substrates: the existence of S dimers will require essentially different adsorption sites or geometries for the dimer's constituents which is obviously not the case. Additional support for individual bonding comes from the experiments on SAMs formed from ADDS (Cn–C16), where a highly disordered film comprised of the AT chains of different lengths can be intuitively expected. The C1s NEXAFS spectra of the Cn–C16 films for an incidence angle of 55° and the differences of the spectra taken at 90° and 20° are shown in figures 17(a) and (b), respectively, in comparison with the analogous spectra for conventional C18 and C12 SAMs. The Cn–C16 and Cn results are very similar. The most pronounced spectral features in figure 17(a) are the characteristic sharp R* resonance at ∼287.7 eV and the broader C–C and C–C′ σ^* resonances at 293.4 eV and 302 eV, respectively. The similar amplitudes of the anisotropy peaks for the Cn–C16 films and C18/C12 SAMs imply that both the orientational order and the average tilt angle of the alkyl chains in the former films and in SAMs comprising the molecules of equal lengths are essentially the same. This indicates that a homogeneously intermixed Cn/C16 overlayer is not the correct model for SAMs formed from Cn–C16. Also note that the intensity of the R* resonance for these SAMs in the original NEXAFS spectra in figure 17(a) exceeds that for the C12 films. Considering that at an incidence angle of 55° intensities of NEXAFS resonances are independent of the molecular orientation [84] and that the intensity of the R* resonance is larger for the AT SAMs consisting of longer alkyl chains [26], the average chain length in the Cn–C16 films seems to be larger than that in the C12 SAM. This is quite unexpected considering that for homogeneously intermixed or phase-separated C4–C16 and C8–C16 films this value should correspond to C10 and C12, respectively. This situation is clarified by examination of the XPS data.

The C 1s and S 2p XPS spectra of the Cn–C16 film and C16 SAMs are shown in figures 18(a) and (b), respectively. For all Cn–C16 films, a single C 1s peak is observed with the BE and FWHM close to those for C16 [52]. The C 1s intensities for the Cn–C16 samples differ only by about 1% from each other, while the carbon content of the respective asymmetric disulphide species differs by about 30%. The C 1s intensity for C16 is by ∼5% higher than those of the Cn–C16 films.

In the S 2p spectra of both Cn–C16 films and the C16 SAM, a single S 2p doublet at ∼162.0 eV (S $2p_{3/2}$) is observed with a FWHM of the S $2p_{3/2}$ and S $2p_{1/2}$ peaks (1.32 eV) close to that for C16 (1.16 eV). The S 2p intensities for the Cn–C16 films are only slightly less than that for C16. The respective BE coincides with that for C16, but differs significantly from the relative value for sulphur in diaminodiphenyl– and dialkyl–disulphides (163.2–163.5 eV

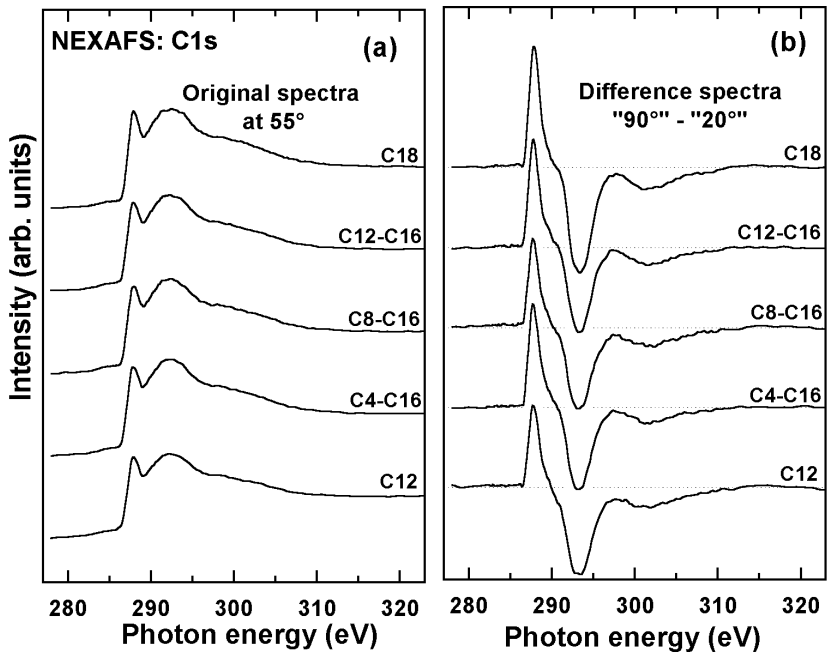

Figure 17. C1s NEXAFS spectra acquired at an incidence angle of 55° for SAMs formed from C12, Cn-C16, and C18 (a) and the respective differences of the NEXAFS spectra taken at incidence angles of 90° and 20° (b).

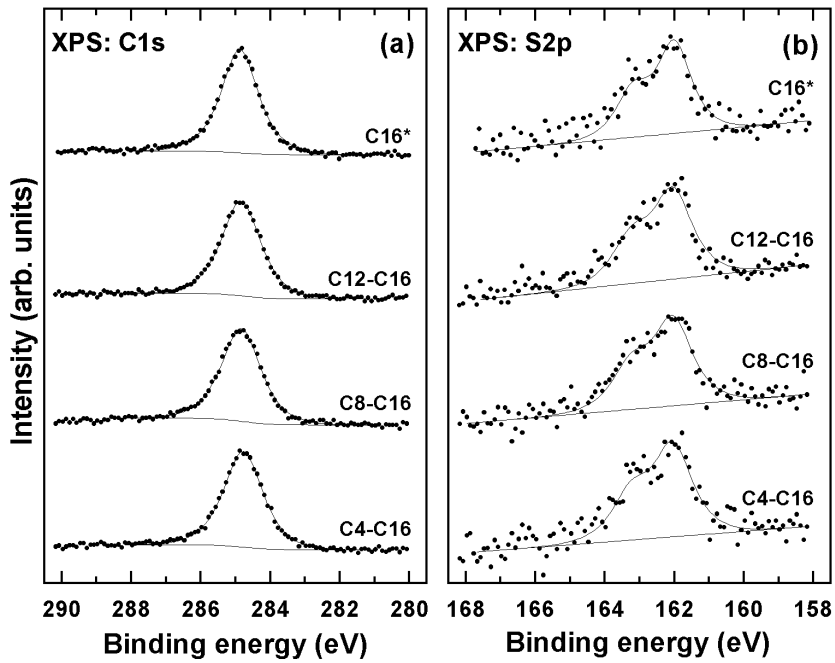

Figure 18. C 1s (a) and S 2p (b) XPS spectra of SAMs formed from C16 and Cn-C16, the spectra for C16 being derived from the relative spectra for C18 SAM. The measurements were performed with the Mg Kα x-ray source (1254 eV) in normal emission geometry.

for S $2p_{3/2}$ [118–120]), which can be intuitively associated with the cleavage of the S–S bond in Cn–C16 molecules upon adsorption on the Au surface. Note that the coincidence of the S 2p binding energies for SAMs formed from AT and DDS was reported previously [57–59, 63].

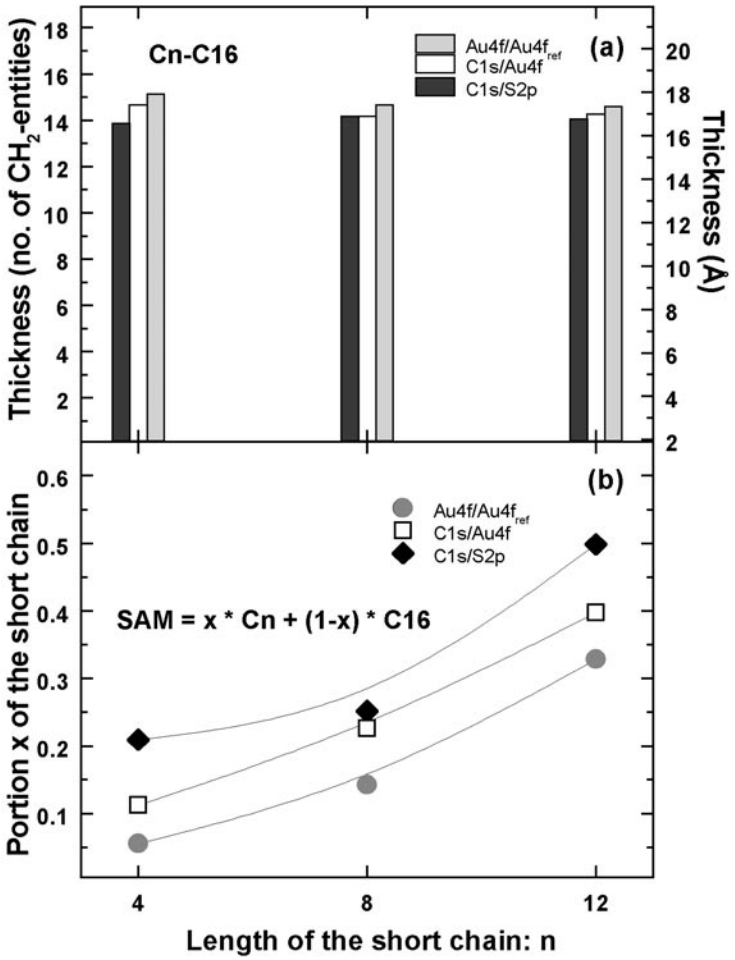

Figure 19. Thickness of the Cn-C16 layers derived from the XPS data in figure 19 (a) and a relative portion of the short chains in these layers (b). The accuracy of the relative portion values is ±0.1.

From the XPS data the thickness of the SAM formed from Cn–C16 was estimated using the C1s/S2p and C1s/Au4f, and Au4f/$Au4f_{ref}$ intensity ratios. The resulting thicknesses are shown in figure 19(a) both in units of Å and methylene entities (m.e.) assuming the chain tilt angle of 33°. Whereas the Au4f/$Au4f_{ref}$, C1s/S2p, and C1s/Au4f derived values differ only slightly, the average thicknesses for all ADDS SAMs, namely 14.6 m.e. (17.4 Å) for C4–C16, 14.4 m.e. (17.1 Å) for C8–C16, and 14.3 m.e. (17.0 Å) for C12–C16 are essentially larger that the values expected for SAMs with equal amounts of Cn and C16 moieties. These results can only be explained assuming that SAMs formed from Cn–C16 consist predominately of C16 chains. This hypothesis agrees also with the presented NEXAFS data and is confirmed by independent IRRAS experiments on SAMs prepared from isotopically labeled ADDS [53]. Analysis of the IRRAS spectra of the mixed SAM prepared from $C_{16}D_{33}S–SC_4H_9$ shows a

composition of ∼92% $C_{16}D_{33}S$– species and ∼8% of C_4H_9S– species on the gold surface. In contrast, for the symmetric $C_{16}D_{33}S$-$SC_{16}H_{33}$ a near 1:1 composition results. All of our results firmly support the existence of a layer comprising mainly of the longer chains in Cn–C16.

The dominance of the C16 chains in SAMs derived from Cn–C16 requires S–S bond cleavage at adsorption of the Cn–C16 molecules on gold surface and the subsequent individual bonding of the Cn and C16 parts to the substrate. Additionally, there is an exchange process resulting in the substitution of shorter chains by longer ones (see [52] for details), with the efficiency increasing with the increasing length difference of the involved chains. In fact, with increasing length of the short chain in the initial Cn–C16 substances the portion of these chains in the Cn–C16 derived SAMs noticeably increases from 5–20% for C4–C16 to 30–50% for C12–C16 (figure 19(b)).

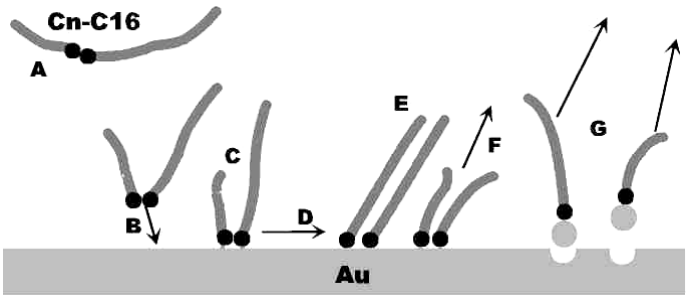

Figure 20. Sketch of the assumed adsorption, desorption, and assembling processes during the immersion of Au substrates in the Cn-C16 solution. See text for explanation.

We assume that the chain substitution process in the present case is essentially mediated by the gold surface, as schematically shown in figure 20 [52]. The alkanethiolate moieties (C), formed initially by S–S bond cleavage of the adsorbing ADDS molecules (A, B), can recombine at the surface (D) to form statistical distributions of symmetric and asymmetric neighbours (C, E and F). One possibility is that short–short disulphides (F) preferentially desorb leaving room for adsorption of more long–short disulphide, thus enriching the monolayer in long chains. It also is possible that the short chains desorb as gold thiolates (G) [121]. The desorption rate for short chain AT SAMs is ∼25% higher than that for long chain ones. Regardless of the specific type, the desorbed species are present at such extremely dilute concentrations that they never effectively compete for readsorption.

5. SAMs as strongly correlated systems

Due to the high orientational order, SAMs represent highly correlated molecular ensembles. One of the examples of the respective phenomena is given in figure 21, where the C 1s spectra of the AT (C12) and BPT SAMs are presented. On both substrates these spectra exhibit a single emission peak with identical FWHMs of 0.76–0.77 eV. In the case of BPT SAMs, this peak is accompanied by a shoulder at ∼1 eV higher BE.

The positions of the C 1s emission for AT and BPT SAMs differ noticeably, which is related to the saturated and unsaturated character of the alkyl and biphenyl moieties, respectively. Another feature of the C 1s spectra is the very similar BEs of the C 1s emission lines for BPT/Au and BPT/Ag and the different BEs of these peaks for AT/Au and AT/Ag. Considering the similarity of the S 2p BEs for the C12 and BPT SAMs (see section 4), this difference cannot stem from different screening of the C 1s hole by the substrate electrons, but might be

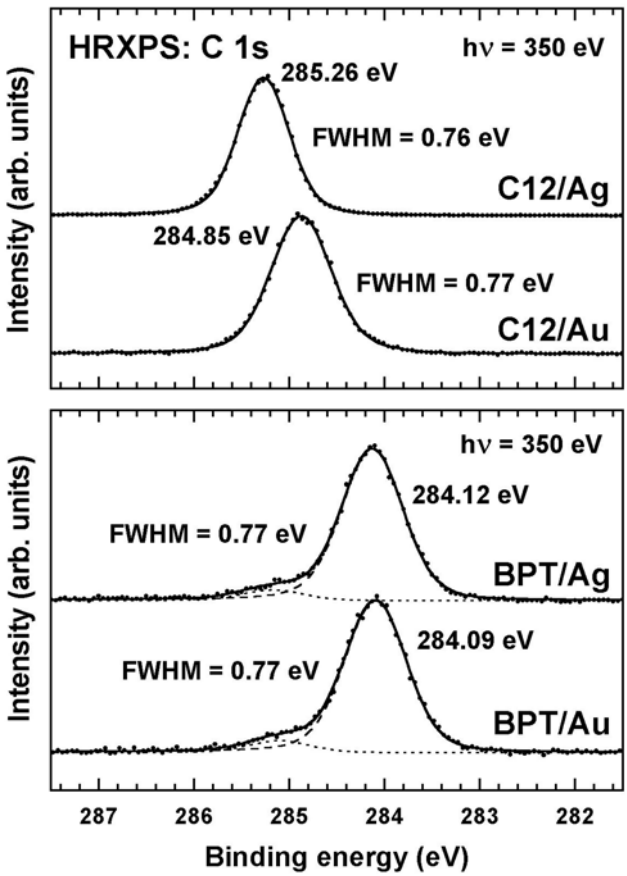

Figure 21. C 1s HRXPS spectra of AT and BPT SAMs on Au and Ag. The BE and FWHM of the main C 1s peak are indicated.

related to the solid-state-like final state effects in the alkyl matrix, which has a denser lateral packing in AT/Ag than in AT/Au. In particular, so-called intersite antiscreening [122], i.e. a transfer of the electron density from the excited molecules to their neighbours might be of importance. Note, that a positive shift of the C 1s peak with increasing lateral packing density was also observed for AT SAMs on Hg-modified Au substrates (see section 3.1 and [33]) and for BPn SAMs on Ag (see figure 6). However, the lack of such a dependence for BPn/Au (see figure 6), which actually have comparable packing densities as BPn/Ag, implies that not only the packing density but also the exact molecular arrangement may affect the BE of the main C1s emission in SAMs.

The higher BE shoulder in the C 1s spectrum for BPT SAMs might be alternatively assigned to the methyl tailgroup, the carbon atom bonded to the sulphur headgroup or to shake-up processes [38, 118, 123]. To make a choice we have to consider the C 1s HRXPS spectra of the BPn SAM in figure 22, where the same shoulder is exhibited (the shoulder is also seen in the corresponding XPS spectra in figure 6). In contrast to the main emission peak, the position of the higher BE shoulder (figure 23(a)) exhibits pronounced odd-even changes for both BPn/Au and BPn/Ag, which on silver are opposite to those on gold. Also the intensity of this shoulder reveals a similar behaviour, as seen in figure 23(b). Considering these odd-even

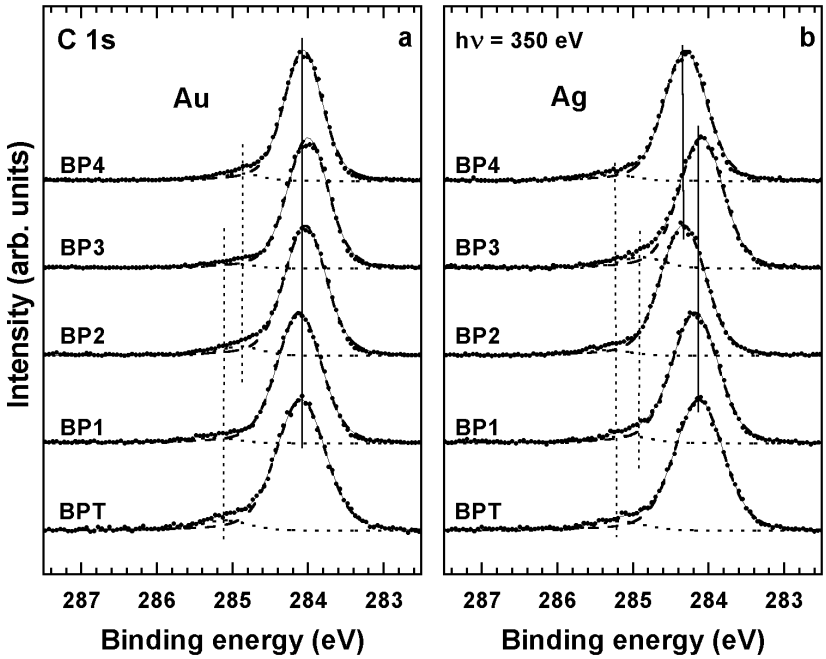

Figure 22. C 1s HRXPS spectra of BPn and BPT SAMs on Au (a) and Ag (b). The positions of the main C 1s peak and the higher BE shoulder are marked by thin solid and dotted lines, respectively. The spectra are normalized to the intensity of the C 1s peak.

effects and their opposite directions for BPn/Au and BPn/Ag, the position and intensity of the higher BE shoulder clearly depends on the density and/or orientation of the biphenyl moieties. Therefore, the shoulder can be assigned to some collective phenomena in the biphenyl matrix, presumably low-energy shake up excitations.

The assignment of this shoulder to shake up processes in the aromatic matrix is also supported by the high surface sensitivity of HRXPS at the given excitation energies: Most of the C 1s signal originates from the biphenyl moieties. The assignment of the shoulder to the carbon atom bonded to the sulphur headgroup or to the methyl tail group does not correlate with it's intensity (see figures 23(b) and 23(c)). First, the absolute intensity of the shoulder does not decrease with the increasing length of the alkyl part, as expected if this feature would originate from the carbon atom bonded to the sulphur headgroup. Second, the average ratio between the intensities of the main C 1s peak and the higher BE shoulder is $\sim$19 as seen in figure 23(c). Considering the strong attenuation of the C 1s photoelectrons in the BPn film at a KE of $\sim$90 eV and a ratio of 13–16 between the number of carbon atoms in the BPn molecules and the aliphatic α-carbon or methyl carbon, a noticeably larger signal than 1:19 (the shoulder with respect to the main C 1s peak) would be expected from the methyl carbons, while a much smaller signal would be proposed for the α-carbons bonded to the sulphur headgroups.

6. Summary

A combination of several complementary spectroscopic techniques, in particular NEXAFS spectroscopy and synchrotron-based HRXPS, was applied to study some principle issues of self-assembly in thiol-derived SAMs. Both conventional aliphatic and aromatic SAMs

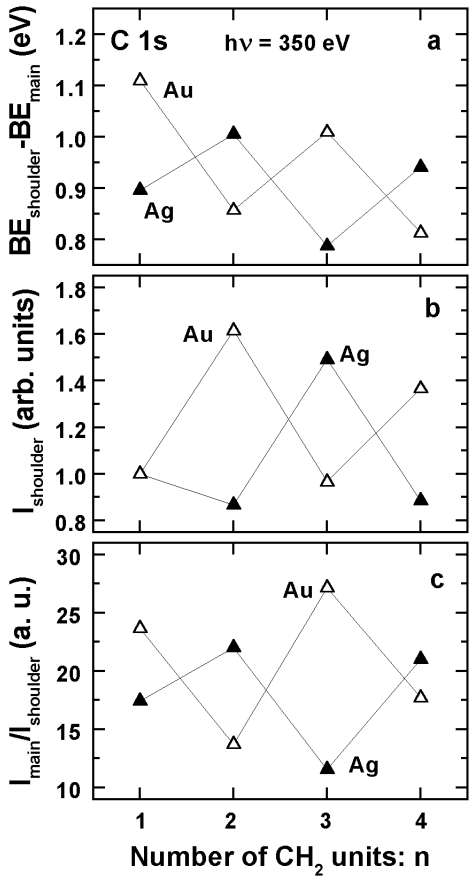

Figure 23. The BE position of the higher BE shoulder with respect to the main C 1s peak (a), the intensity of this shoulder (b), and the ratio between the intensities of the main C 1s peak and the higher BE shoulder (c). The presented values were derived from the C 1s spectra in figure 22. The accuracy of the BE position values is ±0.05 eV.

and several specially designed systems such as SFAT, BPn, AnT, and ADDS films were characterized. It was demonstrated that the balance of structural forces, namely, the headgroup–substrate and intermolecular interactions is different in the aliphatic and aromatic thiol-derived SAMs.

In the aliphatic SAMs, the headgroup–substrate interaction is a decisive factor for the structure and packing of these systems. Not only the corrugation of the sulphur–metal binding energy surface, but also directive forces associated with headgroup–substrate interaction are of a crucial importance, as was shown by the experiments on SFAT and BPn SAMs: the results evidence that a significant driving force exist to pertain the sp^3 and sp hybridization of sulphur headgroups on gold and silver, respectively. Additionally, the decisive influence of the substrate on the structure and packing of the aliphatic SAMs is supported by the structural rearrangement of the AT SAMs on gold after exposure to mercury vapour. This rearrangement can be directly related to the modification of the gold surface due to adsorption/intermixing of mercury on/with gold.

In the aromatic SAMs, the balance between the headgroup/substrate interactions and

the intermolecular forces is shifted toward intermolecular forces. Whereas the thioaromatic molecules in the respective SAMs are less tilted on Ag as compared to Au, the difference in the respective tilt angles is noticeably (by a factor of ∼3) smaller as compared to that for the AT chains in aliphatic SAMs on the gold and silver substrates. In addition, in contrast to AT SAMs, an increase of the number of phenyl rings in thioaromatic molecules, associated with an increase of the intermolecular interactions, results in a less inclined orientation of these molecules in the respective SAMs. Also, a higher molecular rigidity has only a slight effect on the final molecular orientation within the thioaromatic SAMs.

Only one sulphur species could be detected in the S 2p HRXPS spectra of both aliphatic and aromatic SAMs, consistent with a thiolate bond. Another important question on the headgroup–substrate interaction, i.e. whether AT SAMs on gold exist as dimers or individually-bonded AT chains, is answered by the experiments with the ADDS SAMs: the results clearly favour individual bonding as thiolates.

Pronounced chemical shifts in the adsorbate- and substrate-related photoemission lines upon formation of thiol-derived SAM are observed, these shifts being almost identical for the aliphatic and aromatic SAMs. An interesting finding is that whereas the BE differences of the Au 4f/Ag 3d bulk and surface components are distinctly different for the clean Au and Ag surfaces, similar BE differences are observed for both substrates after the adsorption of AT or BBT molecules. This implies a similarity in the character of the headgroup–substrate bonds for the thiol-derived SAMs on both substrates.

Due to the ultimate energy resolution of HRXPS, conclusions on the heterogeneity of the adsorption sites and adsorption geometry in both aliphatic and aromatic SAMs could be made from the FWHMs of the photoemission lines. The obtained spectra are consistent with a superposition of different adsorption sites in the AT films on Ag, and imply several (presumably two) slightly different adsorption geometries in AT/Au in full agreement with the c(4 × 2) modulation of the commensurate $(\sqrt{3} \times \sqrt{3})R30^\circ$ surface lattice. At the same time, such a commensurate lattice of the sulphur headgroups was found in the high quality BPT SAMs and loosely packed BPn SAMs on Au. This 2D arrangement corresponds to a FWHM of the S $2p_{3/2,1/2}$ peaks of ∼0.50 eV, this value is the smallest one found for the thiol-derived SAMs.

During the characterization of different thiol-derived SAMs we found numerous indications that these systems represent highly correlated molecular ensembles. The BE of the main C1s emission in these systems depends both on the packing density of the molecular chains and on their exact arrangement. In the aromatic SAMs, a shake up feature in the C 1s region is observed with the BE position and intensity depending on the packing density of the aromatic matrix. Additionally, a rich variety of mutually related odd-even effects is observed in BPn SAMs.

Except for their relevance for the elucidation of the principle mechanisms of self-assembly, the results obtained for the individual systems are of their own importance. In the case of SFAT SAMs, a lack of information regarding the structure of SFAT films possessing long hydrocarbon segments has been overcome and the structure of the SFAT SAMs on different substrates than Au (the only one studied so far), was investigated. In particular, it was found that the orientation of the fluorocarbon chains in SFAT SAMs does not depend on the substrate and becomes slightly more tilted (or disordered) with increasing length of the hydrocarbon part. In the case of BPn SAMs, a variety of 'odd-even' effects was found. Due to the occurrence of these effects and, especially, due to the possibility to vary the structure and packing density of the BPn films in a controlled way, these films are well suited as model systems for scientific studies and practical applications of SAMs. Also, the AnT monolayers, which were investigated for the first time, are believed to be important for potential application as molecular wires and lithographic

resist material. Finally, in the ADDS SAMs, dissociative chemisorption of the S–S bond upon adsorption and an exchange process involving a subsequent substitution of short chain Cn entities by the longer C16 ones have been found. The data imply a strong dependence of the exchange process on the length difference of the chain parts and on the detailed character of the alkyl substituents.

Acknowledgments

We would like to specially recognize our collaborators Stefan Frey and Karin Heister, who were involved in most of the experiments summarized in this review. Further, we acknowledge Manfred Buck, Michael Himmelhaus, Haitao Rong, Georg Thome, Yong-Jie Yang (all from Angewandte Physikalische Chemie, Universität Heidelberg), Lars Johansson (Karlstad University), Abraham Ulman (Polytechnic University, Brooklyn, USA), David Allara and Kevin Bahnck (Pennsylvania State University, USA), Andreas Terfort and Björn Zeysing (Universität Hamburg), Günter Helmchen (Universität Heidelberg), Christof Wöll and Mario Wühn (Ruhr-Universität Bochum), Kaoru Tamada (RIKEN, Japan), T Randall Lee, Olga E Shmakova, Ramon Colorado, and Michael Graupe (University of Houston, USA) for their cooperation. We would also like to thank Christoff Wöll for providing us with experimental equipment and the MAX II and BESSY staff, especially Mattias Mast for extensive support during the beam times. The work was funded by the Deutsches Ministerium für Bildung und Forschung, Deutsche Forschungsgemeinschaft, Deutscher Akademischer Austauschdienst, and Fonds der Chemischen Industrie.

References

[1] Ulman A 1991 *An Introduction to Ultrathin Organic Films: Langmuir-Blodgett to Self-Assembly* (New York: Academic)
Ulman A 1996 *Chem. Rev.* **96** 1533
[2] Ulman A (ed) 1998 *Thin Films: Self-Assembled Monolayers of Thiols* (San Diego: Academic)
[3] Schreiber F 2000 *Prog. Surf. Sci.* **65** 151
[4] Tour J M, Jones L II, Pearson D L, Lamba J S, Burgin T P, Whitesides G M, Allara D L, Parikh A N and Atre S V 1995 *J. Am. Chem. Soc.* **117** 9529
[5] Bumm L A, Arnold J J, Cygan M T, Dunbar T D, Burgin T P, Jones L II, Allara D L, Tour J M and Weiss P S 1996 *Science* **271** 1705
[6] Geyer W, Stadler V, Eck W, Zharnikov M, Gölzhäuser A and Grunze M 1999 *Appl. Phys. Lett.* **75** 2401
[7] Eck W, Stadler V, Geyer W, Zharnikov M, Gölzhäuser A and Grunze M 2000 *Adv. Mater.* **12** 805
[8] Sabatani E, Cohen-Boulakia J, Bruening M and Rubinstein I 1993 *Langmuir* **9** 2974
[9] Chang S C, Chao I and Tao Y T 1994 *J. Am. Chem. Soc.* **116** 6792
[10] Dhirani A A, Zehner W, Hsung R P, Guyot-Sionnest P and Sita L 1996 *J. Am. Chem. Soc.* **118** 3319
[11] Tao Y T, Wu C C, Eu J Y and Lin W L 1997 *Langmuir* **13** 4018
[12] Himmel H J Terfort A and Wöll Ch 1998 *J. Am. Chem. Soc.* **120** 12 069
[13] Kang J F, Liao S, Jordan R and Ulman A 1998 *J. Am. Chem. Soc.* **120** 9662
[14] Kang J F, Jordan R and Ulman A 1998 *Langmuir* **14** 3983
[15] Kang J F, Ulman A, Liao S and Jordan R 1999 *Langmuir* **15** 2095
[16] Ishida T, Choi N, Mizutani W, Tokumoto H, Kojima I, Azehara H, Hokari H, Akiba U and Fujihira M 1999 *Langmuir* **15** 6799
[17] Leung T Y B, Schwartz P, Scoles G, Schreiber F and Ulman A 2000 *Surf. Sci.* **458** 34
[18] Sellers H, Ulman A, Shnidman Y and Eilers J E 1993 *J. Am. Chem. Soc.* **115** 9389
[19] Taut C, Pertsin A J and Grunze M 1996 *Langmuir* **12** 3481
[20] Pertsin A J and Grunze M 1997 *J. Chem. Phys.* **106** 7343
[21] Laibinis P E, Whitesides G M, Allara D L, Tao Y T, Parikh A N and Nuzzo R G 1991 *J. Am. Chem. Soc.* **113** 7152
[22] Pertsin A J and Grunze M 1994 *Langmuir* **10** 3668

[23] Ulman A, Eilers J E and Tillman N 1989 *Langmuir* **5** 1147
[24] Fenter P, Eisenberger P, Li J, Camillone N III, Bernasek S, Scoles G, Ramanarayanan T A and Liang K S 1991 *Langmuir* **7** 2013
[25] Nuzzo R G, Dubois L H and Allara D L 1990 *J. Am. Chem. Soc.* **112** 558
[26] Hähner G, Kinzler M, Thümmler C, Wöll Ch and Grunze M 1992 *J. Vac. Sci. Technol.* A **10** 2758
[27] Fenter P, Eisenberger P and Liang K S 1993 *Phys. Rev. Lett.* **70** 2447
Fenter P, Eberhardt A and Eisenberger P 1994 *Science* **266** 1216
[28] Walczak M M, Chung C, Stole S M, Widrig C A and Porter M D 1991 *J. Am. Chem. Soc.* **113** 2370
[29] Lampert A 1997 *PhD Thesis* (Universität Heidelberg, Heidelberg, Germany)
[30] Zharnikov M, Frey S, Rong H, Yang Y J, Heister K, Buck M and Grunze M 2000 *Phys. Chem. Chem. Phys.* **2** 3359
[31] Frey S, Heister K, Zharnikov M, Grunze M, Tamada K, Colorado R Jr, Graupe M, Shmakova O E and Lee T R 2001 *Isr. J. Chem.* **40** 81
[32] Rong H T, Frey S, Yang Y J, Zharnikov M, Buck M, Wühn M, Wöll Ch and Helmchen G 2001 *Langmuir* **17** 1582
[33] Thome J, Himmelhaus M, Zharnikov M and Grunze M 1998 *Langmuir* **14** 7435
[34] Lii J H and Allinger N L 1989 *J. Am. Chem. Soc.* **111** 8576
[35] Lide D R (ed) 1991-1992 *CRC Handbook of Chemistry and Physics* 72nd edn (Boston: CRC Press)
[36] Frey S, Stadler V, Heister K, Zharnikov M, Grunze M, Zeysing B and Terfort A 2001 *Langmuir* **17** 2408
[37] Carron K T and Hurley L G 1991 *J. Phys. Chem.* **95** 9979
[38] Whelan C M, Barnes C J, Walker G H and Brown N M D 1999 *Surf. Sci.* **425** 195
[39] Szafranski C A, Tanner W, Laibinis P E and Garrell R L 1998 *Langmuir* **14** 3570
[40] Stern D A, Wellner E, Salaita G N, Laguren-Davidson L, Lu F, Batina N, Frank D G, Zapien D C, Walton N and Hubbard A T 1988 *J. Am. Chem. Soc.* **110** 4885
[41] Gui Y T, Lu F, Stern D A and Hubbard A T 1990 *J. Electroanal. Chem.* **292** 245
[42] Kang J F, Ulman A, Liao S, Jordan R, Yang G and Liu G Y 2001 *Langmuir* **17** 95
[43] Beardmore K M, Kress J D, Gronbech-Jensen N and Bishop A R 1998 *Chem. Phys. Lett.* **286** 40
[44] Grönbeck H, Curioni A and Andreoni W 2000 *J. Am. Chem. Soc.* **122** 3839
[45] Vargas M C, Giannozzi P, Selloni A and Scoles G 2001 *J. Phys. Chem.* B **105** 6888
[46] Fenter P, Schreiber F, Berman L, Scoles G, Eisenberger P and Bedzyk M J 1998 *Surf. Sci.* **412/413** 213
[47] Hutt D A, Cooper E and Leggett G J 1998 *Surf. Sci.* **397** 154
[48] Bensebaa F, Zhou Yu, Deslandes Y, Kruus E and Ellis T H 1998 *Surf. Sci.* **405** L472
[49] Rieley H, Kendall G K, Jones R G and Woodruff P 1999 *Langmuir* **15** 8856
[50] Heister K, Zharnikov M, Grunze M and Johansson L S O 2001 *J. Phys. Chem.* B **105** 4058
[51] Heister K, Rong H T, Buck M, Zharnikov M, Grunze M and Johansson L S O 2001 *J. Phys. Chem.* B **105** 9509
[52] Heister K, Allara D L, Bahnck K, Frey S, Zharnikov M and Grunze M 1999 *Langmuir* **15** 5440
[53] Hooper A E, Heister K, Zharnikov M, Grunze M and Allara D L, to be published
[54] Ishida T, Hara M, Kojima I, Tsuneda S, Nishida N, Sasabe H and Knoll W 1998 *Langmuir* **14** 2092
[55] Biebuyck H A, Bain C D and Whitesides G M 1994 *Langmuir* **10** 1825
[56] Jung Ch, Dannenberger O, Yue Xu, Buck M and Grunze M 1998 *Langmuir* **14** 1103
[57] Nuzzo R G, Zegarski B R and Dubois L H 1987 *J. Am. Chem. Soc.* **109** 733
[58] Bain C D, Biebuyck H A and Whitesides G M 1989 *Langmuir* **5** 723
[59] Dubois L H, Zegarski B R and Nuzzo R G 1993 *J. Am. Chem. Soc.* **98** 678
[60] Schönherr H and Ringsdorf H 1996 *Langmuir* **12** 3891
[61] Biebuyck H A and Whitesides G M 1993 *Langmuir* **9** 1766
[62] Schönherr H, Ringsdorf H, Jaschke M, Butt H J, Bamberg E, Allinson H and Evans S D 1996 *Langmuir* **12** 3898
[63] Ishida T, Yamamoto S, Mizutani W, Motomatsu M, Tokumoto H, Hokari H, Azehara H and Fujihira M 1997 *Langmuir* **13** 3261
[64] Köhn F 1998 *Diploma Thesis* (Universität Heidelberg, Heidelberg, Germany)
[65] Strong L and Whitesides G M 1988 *Langmuir* **4** 546
[66] Bernstorff S, Braun W, Mast M, Peatman W and Schröder T 1989 *Rev. Sci. Instrum.* **60** 2097
[67] Zharnikov M, Frey S, Heister K and Grunze M 2000 *Langmuir* **16** 2697
[68] Batson P E 1993 *Phys. Rev.* B **48** 2608
[69] Moulder J F, Stickle W E, Sobol P E and Bomben K D 1992 *Handbook of X-ray Photoelectron Spectroscopy* ed J Chastian (Eden Prairie: Perkin-Elmer Corp.)
[70] Harder P, Grunze M, Dahint R, Whitesides G M and Laibinis P E 1998 *J. Phys. Chem.* B **102** 426
[71] Band I M, Kharitonov Yu I and Trzhaskoagainstkaya M B 1979 *At. Data Nucl. Data Tables* **23** 443

[72] Yeh J J and Lindau I 1985 *At. Data Nucl. Data Tables* **32** 1
[73] Alves C A and Porter M D 1993 *Langmuir* **9** 3507
[74] Liu G Y, Fenter P, Chidsey C E D, Ogletree D F, Eisenberger P and Salmeron M J J 1994 *J. Chem. Phys.* **101** 4301
[75] Tamada K *et al* 1998 *Thin Solid Films* **327–329** 150
[76] Tamada K, Ishida T, Knoll W, Fukushima H, Colorado R Jr, Graupe M, Shmakova O E and Lee T R 2001 *Langmuir* **17** 1913
[77] Lenk T J, Hallmark V M, Hoffmann C L, Rabolt J F, Castner D G, Erdelen C and Ringsdorf H 1994 *Langmuir* **10** 4610
[78] Tsao M W, Hoffmann C L, Rabolt J F, Johnson H E, Castner D G, Erdelen C and Ringsdorf H 1997 *Langmuir* **13** 4317
[79] Porter M D, Bright T B, Allara D L and Chidsey C E D 1987 *J. Am. Chem. Soc.* **109** 3559
[80] Debe M K 1984 *J. Appl. Phys.* **55** 3354
[81] Ohta T, Seki K, Yokoyama T, Morisada I and Edamatsu K 1990 *Phys. Scr.* **41** 150
[82] Castner D G, Lewis K B, Daniel A F, Ratner B D and Gland J L 1993 *Langmuir* **9** 537
[83] Hähner G, Kinzler M, Wöll Ch, Grunze M, Scheller M K and Cederbaum L S 1991 *Phys. Rev. Lett.* **67** 851
Hähner G, Kinzler M, Wöll Ch, Grunze M, Scheller M K and Cederbaum L S 1992 *Phys. Rev. Lett.* **69** 694 (erratum)
[84] Stöhr J 1992 *NEXAFS Spectroscopy (Springer Series in Surface Science 25)* (Berlin: Springer)
[85] Bagus P S, Weiss K, Schertel A, Wöll Ch, Braun W, Hellwig C and Jung C 1996 *Chem. Phys. Lett.* **248** 129
[86] Weiss K, Bagus P S and Wöll Ch 1999 *J. Chem. Phys.* **111** 6834
[87] Väterlein P, Fink R, Umbach E and Wurth W 1998 *J. Chem. Phys.* **108** 3313
[88] Outka D A, Stöhr J, Rabe J P and Swalen J D 1988 *J. Chem. Phys.* **88** 4076
[89] Piseri L, Powell B M and Dolling G 1973 *J. Chem. Phys.* **58** 158
[90] Castner D L, Gamble L, Fisher D A and Ravel B, to be published
[91] Trotter J 1961 *Acta Crystallogr.* **14** 1135
[92] Charbonneau G P and Delugeard Y 1976 *Acta Crystallogr.* B **32** 1420
[93] Rietveld H M, Maslen E N and Clews C J B 1970 *Acta Crystallogr.* B **26** 693
[94] Harris A L, Rothberg L, Dubois L H, Levinos N J and Dhar L 1990 *Phys. Rev. Lett.* **64** 2086
[95] Yokoyama T, Seki K, Morisada I, Edamatsu K and Ohta T 1990 *Phys. Scr.* **41** 189
[96] Oji H, Mitsumoto R, Ito E, Ishii H, Ouchi Y, Seki K, Yokoyama T, Ohta T and Kosugi N 1998 *J. Chem. Phys.* **109** 10 409
[97] Ågren H, Vahtras O and Carravetta V 1995 *Chem. Phys.* **196** 47
[98] Carravetta V, Ågren H, Pettersson L G M and Vahtras O 1995 *J. Chem. Phys.* **102** 5589
[99] Horsley J A, Stöhr J, Hitchcock A P, Newbury D C, Johnson A L and Sette F 1985 *J. Chem. Phys.* **83** 6099
[100] Weiss K, Gebert S, Wühn M, Wadepohl H and Wöll Ch 1998 *J. Vac. Sci. Technol.* A **16** 1017
[101] Friend C M and Roberts J T 1988 *Acc. Chem. Res.* **21** 394
[102] Stöhr J and Outka D A 1987 *Phys. Rev.* B **36** 7891
[103] Kitaigorodskii I A 1961 *Organic Chemical Crystallography* (New York: Consultants Bureau)
[104] Cruickshank D W J 1956 *Acta Crystallogr.* **9** 915
[105] Culbertson R J, Feldman L C, Silverman P J and Boehm H 1981 *Phys. Rev. Lett.* **47** 675
[106] Citrin P H, Wertheim G K and Baer Y 1983 *Phys. Rev.* B **27** 3160
[107] Hsieh T C, Shapiro A P and Chiang T C 1985 *Phys. Rev.* B **31** 2541
[108] Andersen J N, Hennig D, Lundgren E, Methfessel M, Nyholm R and Scheffler M 1994 *Phys. Rev.* B **50** 17 526
[109] Wöll Ch, Chiang S, Wilson R J and Lippel P H 1989 *Phys. Rev.* B **39** 7988
[110] Yeganeh M S, Dougal S M, Polizzotti R S and Rabinowitz P 1995 *Phys. Rev. Lett.* **74** 1811
[111] Himmelhaus M, Gauss I, Buck M, Eisert F, Wöll Ch and Grunze M 1998 *J. Electron Spectrosc. Relat. Phenom.* **92** 139
[112] Beamson G and Briggs D 1995 *High Resolution XPS of Organic Polymers* (Chichester: Wiley)
[113] Jaffey D M and Madix R J 1994 *Surf. Sci.* **311** 159
[114] Chenakin S P, Heinz B and Morgner H 1999 *Surf. Sci.* **421** 337
[115] Camillone N III, Chidsey C E D, Liu G and Scoles G 1993 *J. Chem. Phys.* **98** 3503
Camillone N III, Chidsey C E D, Liu G and Scoles G 1993 *J. Chem. Phys.* **98** 4234
[116] Poirier G E and Tarlov M J 1994 *Langmuir* **10** 2853
[117] Delmarche E, Michel B, Biebuyck H A and Gerber C 1996 *Adv. Mater.* **8** 719
[118] Gölzhäuser A, Panov S, Schertel A, Mast M, Wöll Ch and Grunze M 1995 *Surf. Sci.* **334** 235
[119] Wirde M, Gelius U, Dunbar T and Allara D L 1997 *Nucl. Instrum. Methods. Phys. Res.* B **131** 245
[120] Heister K, Zharnikov M, Grunze M, Johansson L S O and Ulman A 2001 *Langmuir* **17** 8

[121] Edinger K, Grunze M and Wöll Ch 1997 *Ber. Bunsenges. Phys. Chem.* **101** 1811
[122] Schirmer J, Angonoa G, Svensson S, Nordfors D and Gelius U 1987 *J. Phys. B: At. Mol. Phys.* **20** 6031
[123] Whelan C M, Smyth M R and Barnes C J 1999 *Langmuir* **15** 116